RECEIVED
LAWRENCE
RADIATION LABORATORY

TECHNICAL INFORMATION SECTION

UCRL-19665 c. 2
UC-37 Instruments
TID-4500 (56th Ed.)

CALIBRATION OF AN INFRARED PYROMETER

G. A. McCoy,* R. A Olstad and D. R. Olander

September 1970

AEC Contract No. W-7405-eng-48

*Filed as a Master's Thesis

TWO-WEEK LOAN COPY

This is a Library Circulating Copy which may be borrowed for two weeks. For a personal retention copy, call Tech. Info. Division, Ext. 5545

LAWRENCE RADIATION LABORATORY
UNIVERSITY of CALIFORNIA BERKELEY

UCRL-19665 c. 2

DISCLAIMER

This document was prepared as an account of work sponsored by the United States Government. While this document is believed to contain correct information, neither the United States Government nor any agency thereof, nor the Regents of the University of California, nor any of their employees, makes any warranty, express or implied, or assumes any legal responsibility for the accuracy, completeness, or usefulness of any information, apparatus, product, or process disclosed, or represents that its use would not infringe privately owned rights. Reference herein to any specific commercial product, process, or service by its trade name, trademark, manufacturer, or otherwise, does not necessarily constitute or imply its endorsement, recommendation, or favoring by the United States Government or any agency thereof, or the Regents of the University of California. The views and opinions of authors expressed herein do not necessarily state or reflect those of the United States Government or any agency thereof or the Regents of the University of California.

TABLE OF CONTENTS

I. METHODS OF TEMPERATURE MEASUREMENT

A. Electrical Devices ---------- 1

B. Optical Devices ---------- 2

C. Infrared Pyrometer ---------- 4

II. PHOTODIODE CHARACTERISTICS

A. General Description ---------- 5

B. Detector Response ---------- 8

III. THE INFRARED PYROMETER

A. Description ---------- 15

B. Effect of Source-to-Pyrometer Distance ---------- 18

C. Spot Size ---------- 18

D. Correction for Hole Size and Temperature of Surroundings ---------- 21

E. Determination of Emissivity ---------- 26

F. Temperature Measurement of a Plane Surface ---------- 27

IV. CALIBRATION

A. Below 1000°C ---------- 28

B. Above 1000°C

1. Emissivity of Hole ---------- 28

2. Emissivity of Cavity ---------- 32

3. Non-blackness Correction ---------- 32

C. Calibration Conditions ---------- 33

V. THEORETICAL OUTPUT VS. TEMPERATURE ---------- 34

VI. RESPONSE TIME ---------- 40

Appendix A. Cassegrain Lens System: Theoretical Spot Size ----- 44

Appendix B. Calibration Curves ---------- 48

Bibliography ---------- 55

UCRL-19665

CALIBRATION OF AN INFRARED PYROMETER

G. A. McCoy,* R. A. Olstad and D. R. Olander

Inorganic Materials Research Division, Lawrence Radiation Laboratory,
Department of Nuclear Engineering, College of Engineering,
University of California, Berkeley, California

ABSTRACT

The purpose of this work was to investigate the behavior of an InSb infrared pyrometer and obtain a calibration curve in the temperature range 200°C to 2200°C. The detector responds to radiation in the 2 - 6μ range.

At temperatures below 1000°C the calibration was carried out using a commercial black body source. For calibration above 1000°C, two graphite black body configurations were used, and calibration consisted of matching the infrared pyrometer signal with the corresponding temperature measured by an optical pyrometer.

All calibrations are for a black body hole 0.156 inches diameter with room temperature surroundings, at a pyrometer-to-source distance of 24 inches. A correction factor was derived for black body holes of various sizes with surroundings hot enough to contribute to the detector signal.

A response time of less than 10μ sec was measured. The repeatability varied from ±2°C at low temperatures to ±8°C at 2000°C. The uncertainty is largely due to the operator's skill in aligning the instrument. An error at higher temperatures is due to the uncertainty in the optical pyrometer measurements.

A comparison between the theoretically predicted signal and measured signal was made. Agreement was within 5°C at low temperatures.

---

* In partial fulfillment for M. S. Degree, U. C. at Berkeley, Sept. 1970.

I. METHODS OF TEMPERATURE MEASUREMENT

An accurate knowledge of the temperature at which a particular phenomenon occurs is necessary in many experiments. In light of this, several methods of making high temperature measurements have been developed, some of which have advantages in particular situations.

A. Electrical Devices

The thermocouple is a popular temperature measuring device consisting of two dissimilar wires joined together to form a loop. If the junctions are held at different temperatures, an emf will be generated. Thermocouples are simple, relatively inexpensive, can measure wide temperature ranges and can be readily connected to many types of indicating or controlling devices. Disadvantages are aging, an upper temperature limited by existing thermocouple materials and a large mass which causes response-speed problems. Since electrical connections must be made to the thermocouples, they are not suited for applications involving moving objects. In addition, the temperature of the junction may vary from the temperature being measured, especially in surface-temperature measurements.[1]

The thermistor, or thermally sensitive resistor, generally has a temperature span in the neighborhood of 200°C, and has its greatest use below 300°C. High sensitivity (i.e. large resistance changes per degree of temperature) can be combined with very small thermistor beads to give low heat capacity and fast response. Thermistors avoid reference junction compensation difficulties, polarity checks, and lead-length compensations.[1]

B. Optical Devices

Optical devices are those in which the measurement depends upon the radiant energy emitted by the hot source. The radiant energy emitted by a black body is given by Planck's Law

$$J_{b\lambda} = \frac{C_1}{\lambda^5(\exp \frac{C_2}{\lambda T} - 1)} \tag{1}$$

where $J_{b\lambda}$ is the amount of energy radiated at wavelength λ per unit area and per unit time, and T is the absolute temperature of the radiator. C_1 and C_2 are the first and second radiation constants.

In the visible range, for temperatures less than 3000°K, Wien's approximation may be used

$$J_{b\lambda} \cong C_1\lambda^{-5} \exp(-C_2/\lambda T) \tag{2}$$

Most real surfaces are not perfect emitters; the emission from a non-black surface may be expressed in terms of black-body emission by

$$J_\lambda = \varepsilon_\lambda J_{b\lambda} \tag{3}$$

The spectral emissivity ε_λ is a function of wavelength and temperature. Emissivity is generally thought of as being a bulk or material property, a property of an ideal body. In practice, surfaces are not optically flat, and in addition may contain some film or oxide. The term "emittance" is used to describe this non-ideal state. Emittance is not a constant characteristic of the material. It refers to the material surface at the time of observation and under specific environmental conditions.

A brightness or optical pyrometer measures the temperature by comparing the apparent brightness or flux of radiant energy of a hot object with the known brightness of a calibrated filament. One of the major disadvantages of an optical pyrometer is that the emittance of the target object must be known. Another is the requirement of a human operator.

A ratio or two-color pyrometer makes two brightness temperature measurements using two wavebands of energy. Since the emittance of most surfaces varies slowly with wavelength, the ratio of the two measurements is relatively unaffected by the emittance of the object. Using Eq. (2) at λ_1 and λ_2:

$$R = \frac{J_{\lambda_1}}{J_{\lambda_2}} = \frac{\varepsilon_1 C_1 \lambda_1^{-5} \exp\left(-C_2/\lambda_1 T\right)}{\varepsilon_2 C_1 \lambda_2^{-5} \exp\left(-C_2/\lambda_2 T\right)} \tag{4}$$

If the emissivities at the two wavelengths are equal, the ratio R depends entirely on T, the desired temperature. A typical ratio pyrometer uses one photomultiplier to detect the intensity at two wavelengths. A filter rotates in front of the photomultiplier, alternately admitting red and blue light.

The ratio pyrometer concept minimizes the problem of emittance and eliminates this problem entirely for gray bodies. Electronic sensing also eliminates the requirement of an operator. However, both optical and ratio pyrometers have a limited response time. In addition, neither can be used below approximately 750°C, since the intensity in the visible region is not sufficient for comparison below that temperature.

C. Infrared Pyrometers

In some applications, none of the above temperature measuring devices are adequate. One such instance is the measurement of the surface temperature of a rapidly rotating disk. The thermocouple or thermistor cannot be attached to the disk because of its motion. The optical pyrometer cannot be used below 750°C.

A second instance involves the rapid heating of solid surfaces by a laser pulse. Since the laser pulse and resultant temperature transient are in the millisecond range, a detector with a fast response time is required.

A semiconductor infrared pyrometer, with its fast response time (microsecond time constant as compared to one hundredth of a second for a thermocouple), wide temperature range, and ability to determine surface temperatures directly is ideal for these applications.

II. PHOTODIODE CHARACTERISTICS

A. General Description

Semiconductor detectors generally work in two modes - photoconductive and photovoltaic.[2] In a photovoltaic detector, an electric field is built into the detector by way of a p-n junction. Photons incident on the junction create hole-electron pairs which are separated by the action of the field before they can recombine, thus establishing a current source.*

For a photovoltaic indium antimonide photodiode used in the detector described here, photons with energy greater than the band gap will create electron-hole pairs. The holes, if created within the diffusion length to the junction, flow to and fall down the potential hill to the p side. The electrons remain in the n region and eventually recombine, the net effect being a current flow across the junction.[3]

The InSb photodiode is prepared by the reaction of purified stoichiometric proportions of indium and antimony. The compound is grown into single crystals, and elements of the desired dimensions are then cut from the crystal. The sensitive p-n junction is formed by diffusing p-type impurities onto the surface of the n-type InSb crystal.[2] The photodiode used here is the Philco-Ford Corp. model L4540.[4] The diode is mounted in a small vacuum dewar to permit cooling to liquid nitrogen temperature.

---

* An external battery maintains a current in a photoconductive detector. In this mode no p-n junction is needed, just a semiconductor. Incident photons free additional change carriers from atoms of the crystal when valence electrons are raised to the conduction band.

When examining a detectivity* versus wavelength plot for indium antimonide (Fig. 1), it is found that the maximum response lies between two and six microns. According to Wien's displacement law,

$$\lambda_{MAX} \cdot T = 2897.6\mu^{\circ}K \tag{5}$$

the maximum of the Planck distribution falls within the photodiode spectral range in the temperature interval between 500 and 1500°K. The InSb photodiode can be used for temperatures above 200°C.

* The detectivity is defined as the signal to noise ratio per watt of incident power.

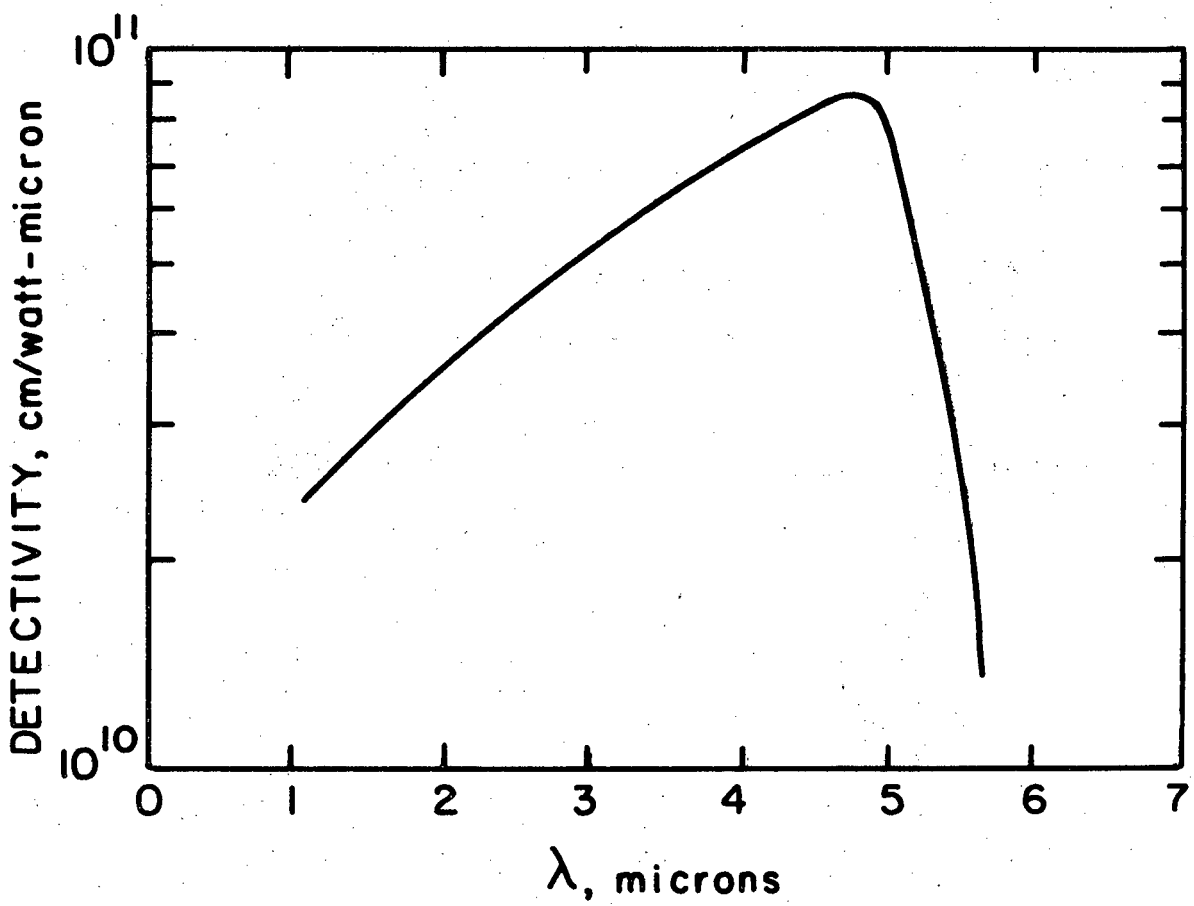

XBL 708-1910

Fig. 1. Detectivity of InSb diode at 77°K as a function of wavelength. Curve taken from Philco-Ford Product Sheet EO-112.

B. Detector Response

Typically, the detector is connected in a circuit such as that shown in Fig. 2. The output voltage signal depends upon the I-V characteristics of the diode and upon the external circuit. The diode I-V characteristic is given by[5]

$$I = -I_{sc} + I_s \left[\exp\left(\frac{eV}{kT_d}\right) - 1 \right] + V/R_{diode} \qquad (6)$$

where I is the current through the circuit, V is the voltage across the diode and I_{sc} is the current source due to the incident radiation from the hot target. I_s is the reverse saturation current and R_{diode} is the diode resistance. Both are peculiar to the particular diode. T_d is the temperature of the detector (usually 77°K). The electronic charge is denoted by e and k is the Boltzmann constant.

The load line of the external circuit is determined by:

$$V = -IR + V_o \qquad (7)$$

The operating point is the intersection of the I-V curve with the load line. Typical situations are shown in Fig. 3. In the present experiments, no bias voltage was employed ($V_o = 0$) and load resistors of 1k, 10k, and 100k were used.

The I-V characteristic curve of the present detector with 300°K background radiation impinging on the diode is shown in Fig. 4. From this plot and Eq. (6), the diode parameters were found to be:

$$R_{diode} = 20 \text{ M}$$

$$I_s = 6 \times 10^{-14} \text{ amps}$$

T_d was 77°K in these tests.

The current induced by the incident radiation from the hot target

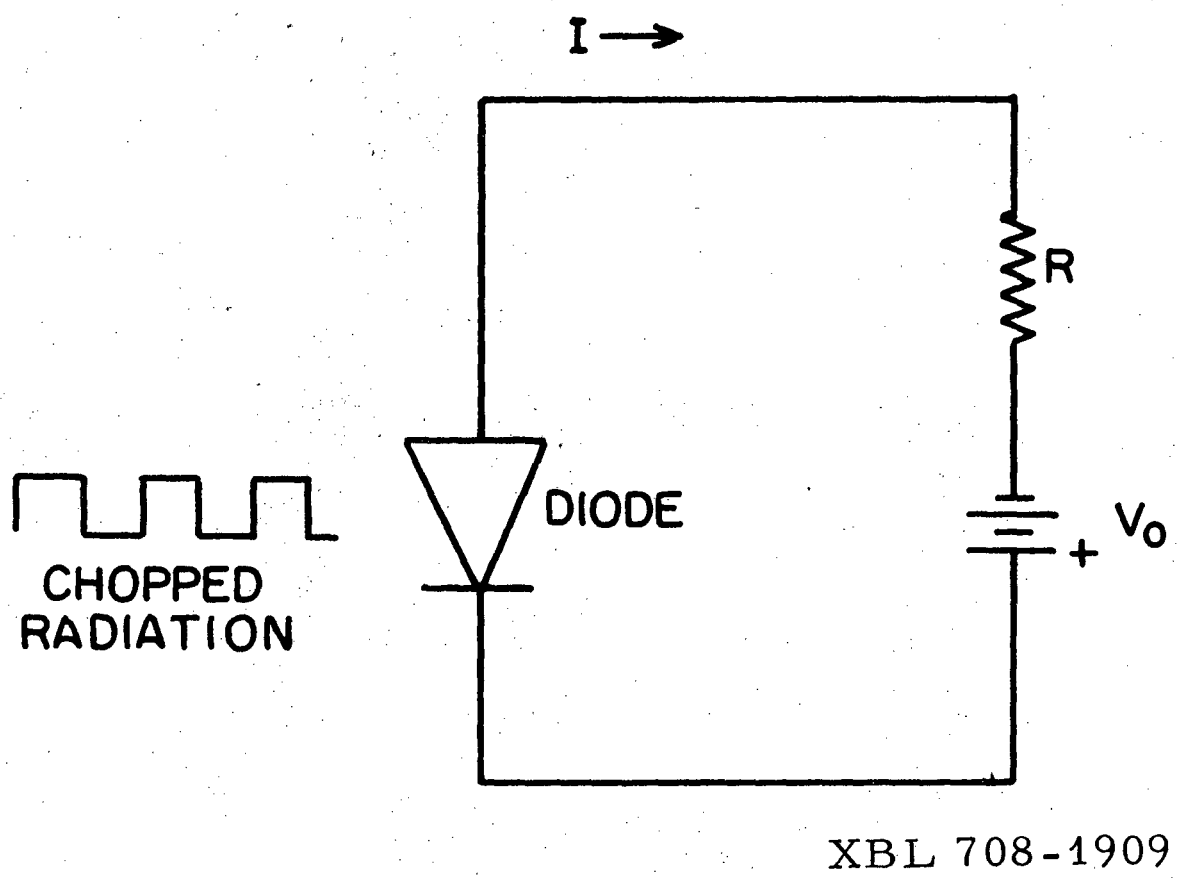

Fig. 2. Typical circuit used with the detector.

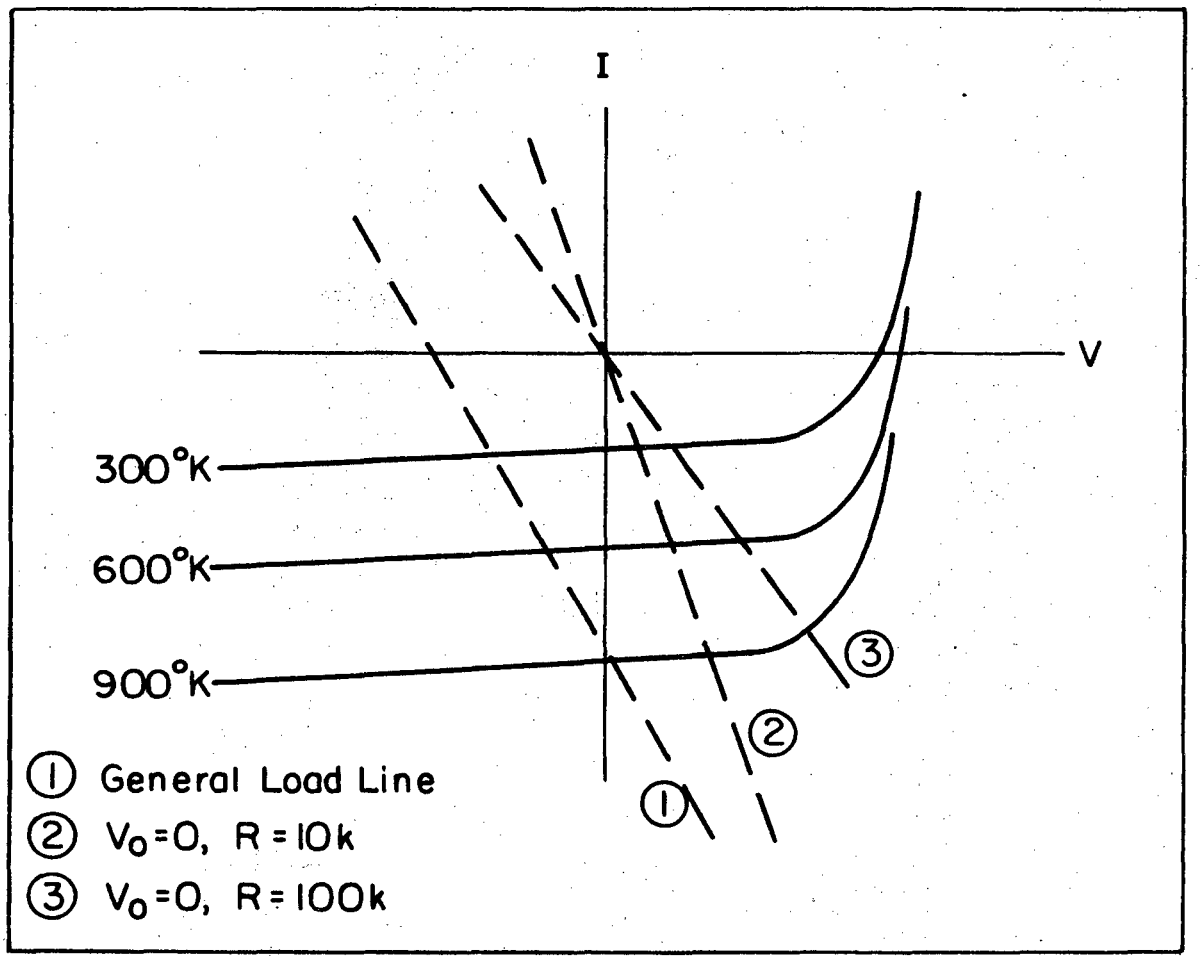

XBL 708-1908

Fig. 3. Typical detector I-V characteristics and load lines.

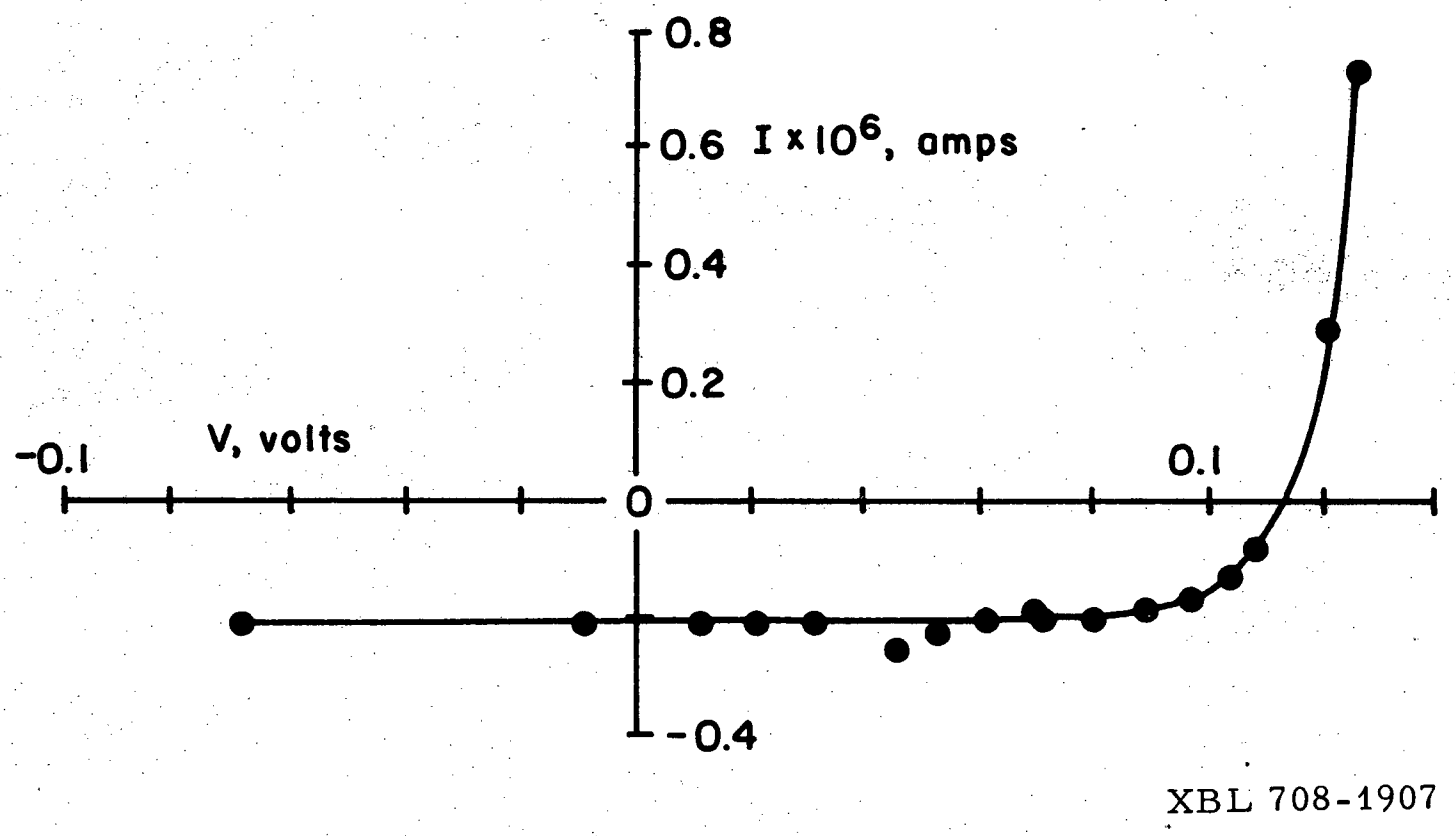

Fig. 4. Measured I-V characteristic curve of InSb detector with 300°K background radiation.

is obtained as follows. Assume that the lens system of the pyrometer views a spot of area A on a hot surface at temperature T. The pyrometer collects radiation over a solid angle $\Delta\Omega$ from the hot target. If ε_λ is the spectral emissivity of the target and U_λ is the number of electron-hole pairs generated by a unit of energy input of photons of wave length λ, the induced current is:

$$I_{sc} = e\int_{\lambda_{min}}^{\lambda_{max}} \varepsilon_\lambda \tau_\lambda U_\lambda J_{b\lambda}(T)\, d\lambda\, \Delta\Omega A \qquad (8)$$

e is the electronic charge and τ_λ is the transmissivity of the elements of the optical system. λ_{max} is the longest wavelength to which the diode responds and is determined by the band gap of the semiconductor material. λ_{min} is the shortest wavelength to which the diode responds. Choice of λ_{min} is somewhat arbitrary, since the detector material simply becomes more transparent as the wavelength decreases. Both λ_{max} and λ_{min} could have been considered as part of the efficiency function U_λ, which has the general shape of the detectivity curve of Fig. 1. An approximate expression for U_λ taken from the curve of Fig. 1 is:

$$U_\lambda \sim \text{constant} \times e^{-a/\lambda} \qquad (9)$$

Using Fig. 1 as a guide, $\lambda_{max} \sim 5.2\mu$, $\lambda_{min} \sim 2\mu$, and $a \sim .3\mu$.

The present system was utilized with operating points essentially on the flat portion of the I-V curves, which implies that the last two terms on the right of Eq. (6) were negligible. Consequently, $I \sim -I_{sc}$, and with no bias voltage ($V_o=0$), the output voltage is:

$$V = I_{sc}R \qquad (10)$$

According to Eq. (10), the output signal should increase rapidly with

source temperature.* This behavior was indeed observed up to the point at which the voltage was large enough to cause the last two terms of Eq. (6) to become significant. This occurrence places the operating points on the steeply rising portion of the I-V curves of Fig. 3 and saturation occurs (i.e., no further increase in signal as the source temperature is increased). At this point it is necessary to switch to a smaller load resistor to get back on the flat portions of the I-V curves, where Eq. (10) is valid and sensitivity to temperature is high. Typical examples of the output-temperature response of the detector are shown in Fig. 5. Saturation for R = 200 k, 100 k, and 50 k is evident. The data represented by these curves are for illustrative purposes only; they are not of calibration quality.

---

* If ε_λ, τ_λ, and U_λ were all constant, the signal would rise as T^4. Detailed consideration of the detector response with temperature is presented in Sec. V.

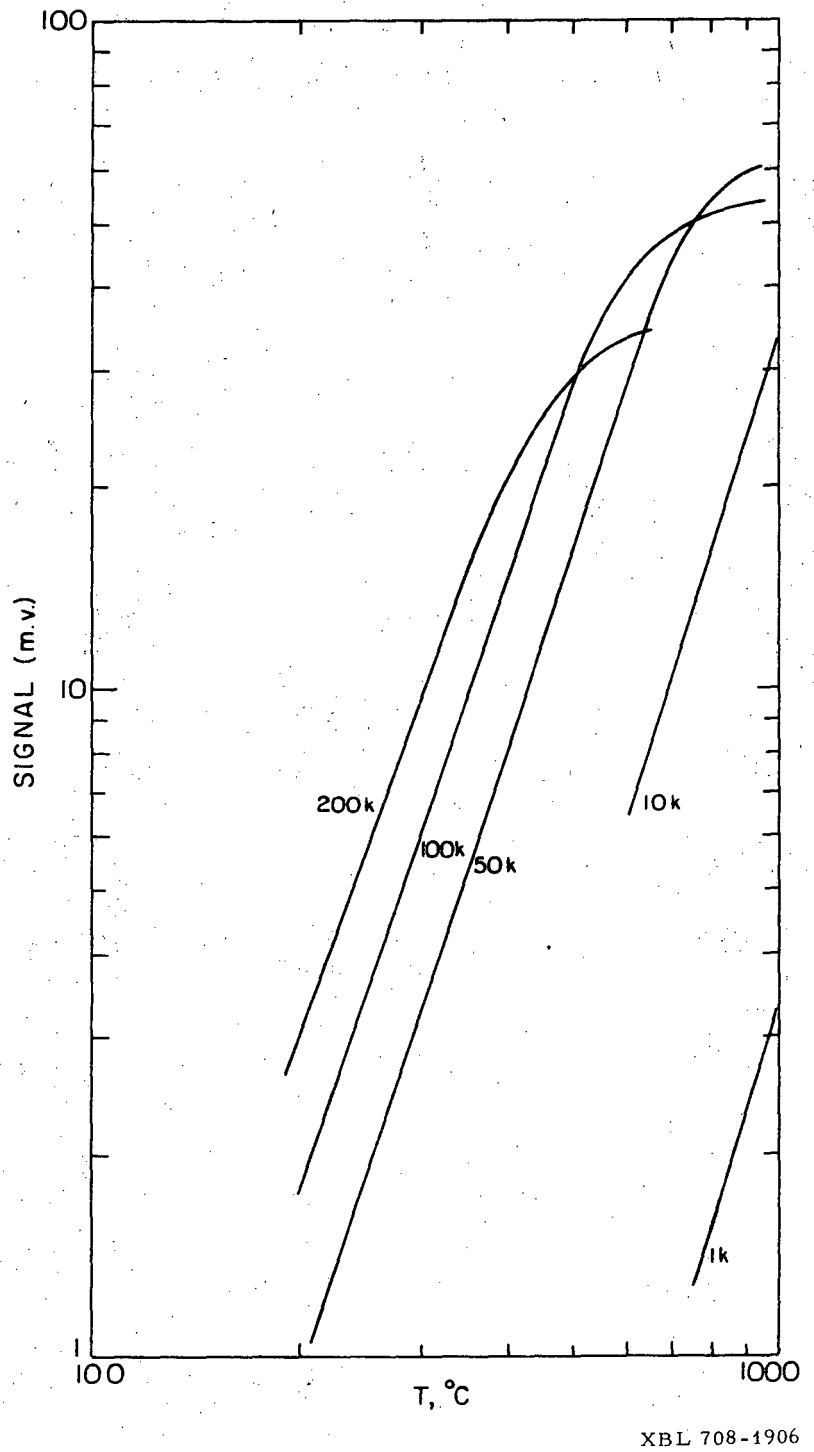

Fig. 5. Detector signal versus source temperature for various load resistances.

III. THE INFRARED PYROMETER

A. Description

A schematic of the pyrometer is shown in Fig. 6. The radiation from the hot target entering from the upper left of the picture is collected by a Cassegrain lens system. The optical characteristics of this lens are discussed in detail in Appendix A. The radiation impinging on the large concave mirror is reflected to a smaller, centrally placed convex mirror which renders the radiation parallel. The beam is turned at right angles by a mirror and strikes a dichroic mirror at 45°. This component acts as a beam splitter. It is made of Kodak IRTRAN-2, which transmits most of the radiation in the 2 - 6μ range of the InSb diode (see Fig. 7 for transmittance curve for IRTRAN-2). Sufficient visible light is reflected from the surface of the beam splitter to the eyepiece for visual focusing on the hot target. At temperatures below 1000°C, however, artificial illumination of the target is necessary to view the surface through the eyepiece. A slight position adjustment of the pyrometer is required to produce the optimum infra-red signal when the unit is aligned visually, since the two alignments do not exactly coincide.

The infra-red radiation transmitted by the beam splitter is mechanically chopped at 60 Hz before being focused by a lens on the 4 mm^2 sensitive area of the InSb detector. The purpose of the modulation of the radiation is to provide signal information in AC form while the unmodulated background radiation which may leak into the diode area and electrical noise in the detector and electronics is DC. The electrical output of the detector is processed by the circuit of Fig. 2. The AC

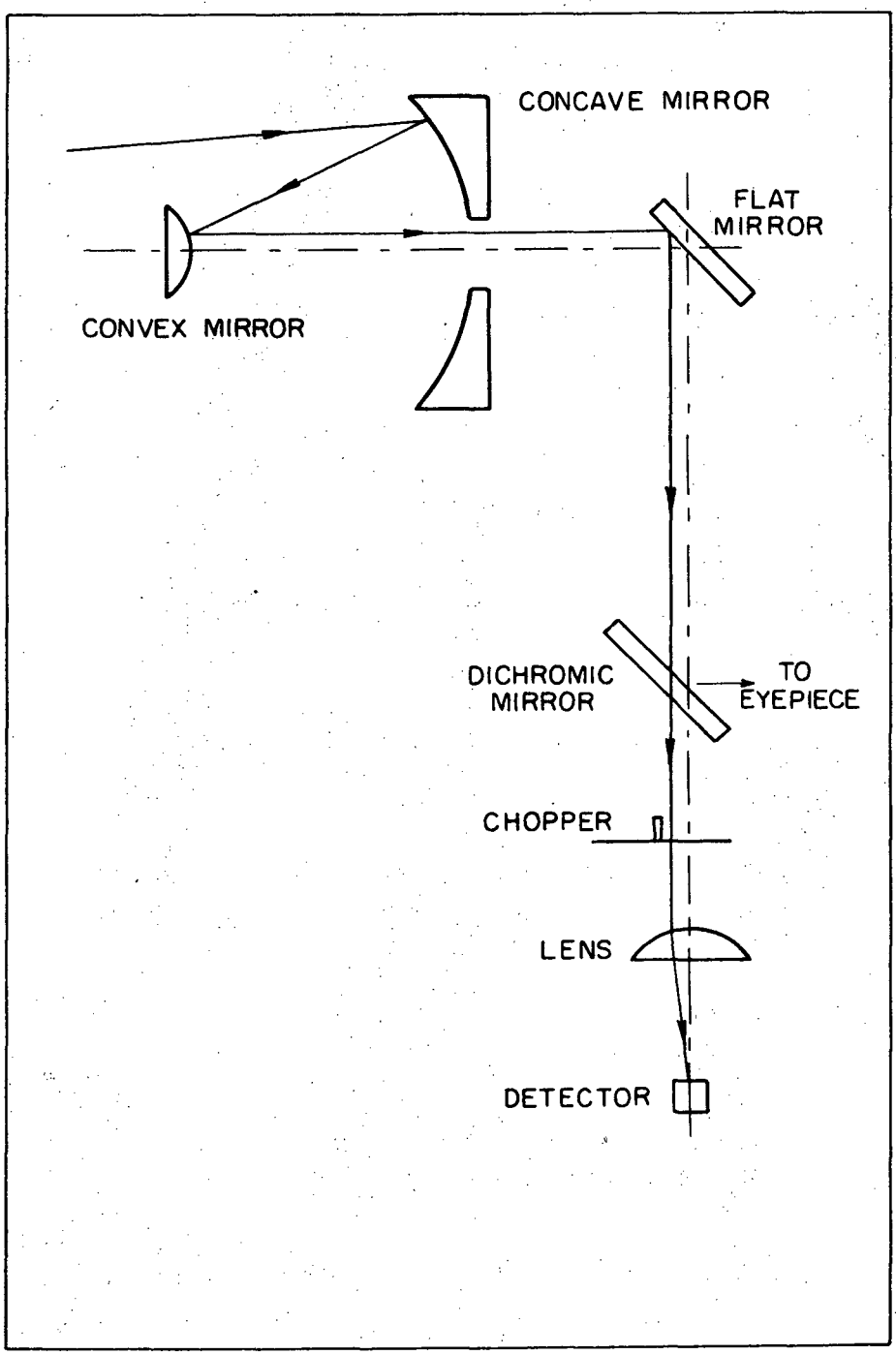

XBL 708-1905

Fig. 6. Infrared pyrometer optical system.

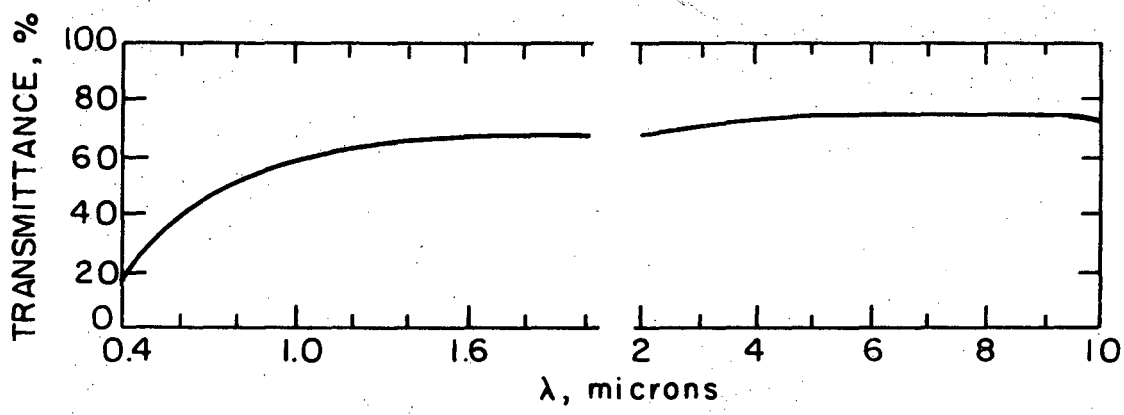

XBL 709-6492

Fig. 7. Transmissivity of IRTRAN-2.

(signal) component of the total output voltage is measured by a digital voltmeter, which produces a signal output (denoted by S) proportional to the amplitude of the AC component of the input (V of Eq. (10). Typical output signal levels are shown in Fig. 5 as a function of target temperature.

B. Effect of Source-to-Pyrometer Distance

The variation of signal with source-to-pyrometer distance is not the same for an infrared radiometer as for an optical pyrometer.

The temperature measured with an optical pyrometer is not dependent on distance from the source since the image formed varies in size so as to just compensate for the $1/\ell^2$ attenuation of source flux (ℓ = source-to-pyrometer distance). Therefore, the energy per unit area per second passing through the plane of the filament is independent of position. This does not hold for the infrared pyrometer since the signal is proportional to the total number of photons impinging on the detector area. Fig. 8 shows the effect of focal distance on the signal for a fixed target temperature. The infrared pyrometer was calibrated for a fixed distance of 24 inches.

C. Spot Size

The area of the radiation source surface viewed by the pyrometer is determined by two parameters:

1. The distance between the mirrors in the Cassegrain optical system (see Appendix A).
2. The distance from the detector to the converging lens just prior to the detector (Fig. 6).

Figure 9 shows that the smallest spot size is obtained when the detector is placed close to the lens. In the present system, the detector was located

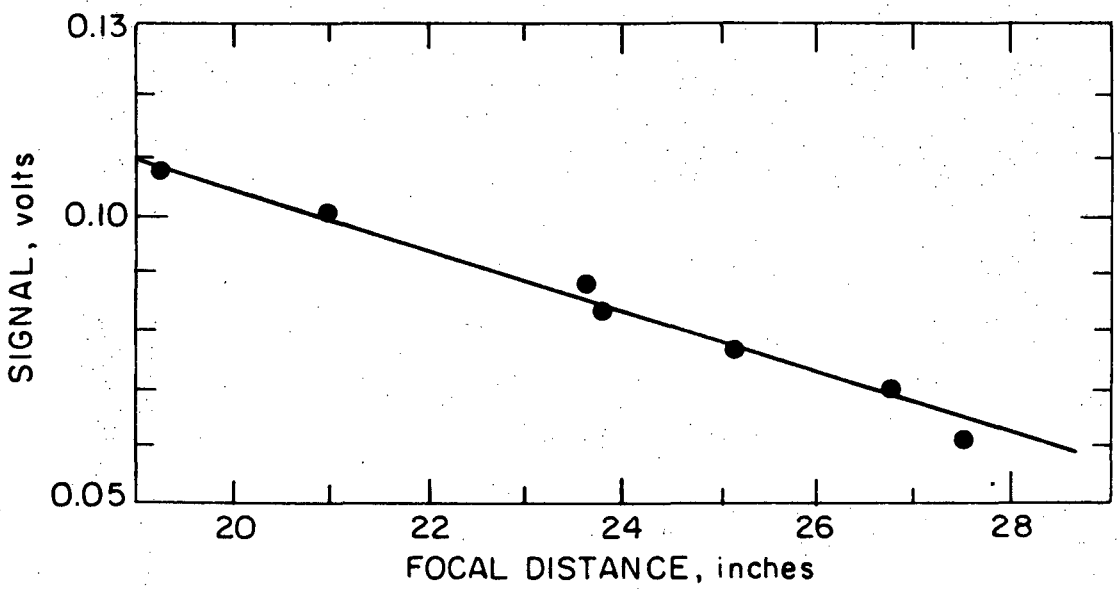

XBL 708-1904

Fig. 8. Effect of source-to-pyrometer distance on the output signal.

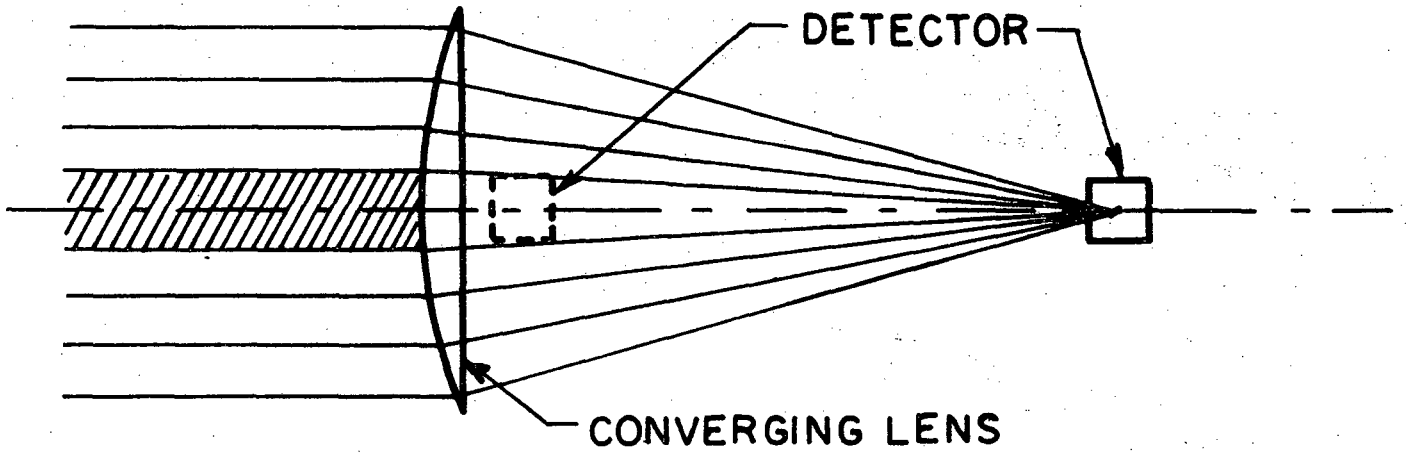

XBL 708-1903

Fig. 9. Effect of detector location on the spot size.

at the focal point in order to obtain the largest possible signal.

With the detector responding to all radiation collected, the spot diameter at the source was calculated to be 0.11 inches (Appendix A). This result was verified qualitatively by sweeping the pyrometer over a small (0.025 in. diam.) black-body hole. The vertical and horizontal sweeps gave widths on the order of 0.04 in. and 0.06 in. respectively (the total widths of the curves in Figs. 10 and 11 less the hole diameter) The area of the hot target viewed by the pyrometer is this somewhat elliptical in shape.

D. Correction for Hole Size and Temperature of Surroundings

In many applications, the pyrometer may be set to view a hole smaller than the one required for maximum pyrometer signal. The measured signal may therefore contain a contribution from the surroundings of a hot hole (which may be at a different temperature or have a different emissivity) in addition to the signal from the hot hole proper. This effect is demonstrated by focusing the pyrometer on black body holes of successively larger diameter. The plot of Fig. 12 shows the results of this test. The maximum signal was obtained with the largest hole available on the commercial black body source (3/8 in. diam.). This reading appears to be close to the signal which would have been obtained from an infinitely large surface (or hole), and is denoted by S_∞. It was noted that the signals from smaller holes, denoted by S, were related to the maximum signal by the relation:

$$\frac{S}{S_\infty} = \frac{1}{1+\Delta} \qquad (11)$$

where the correction factor Δ depends upon the diameter of the black

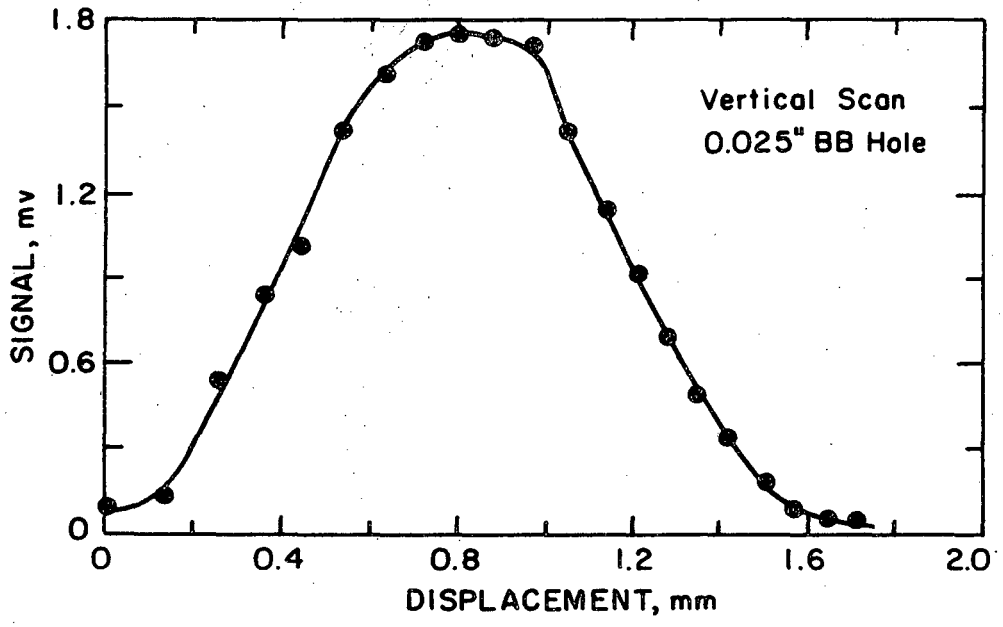

Fig. 10. Pyrometer signal as function of vertical position of a 0.025 in. diameter black body hole.

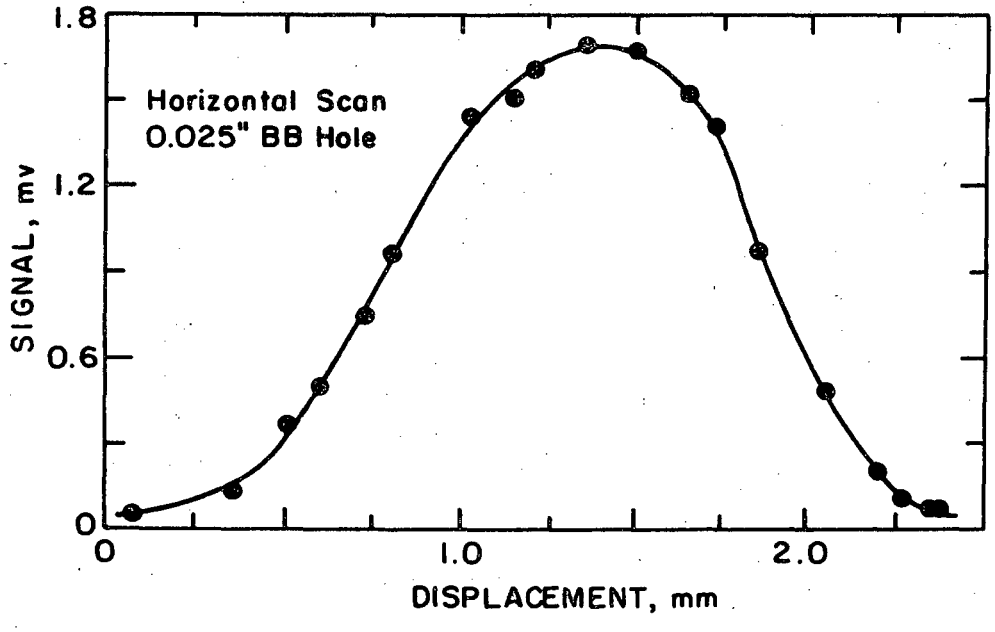

XBL 708-1902

Fig. 11. Pyrometer signal as function of horizontal position of a 0.025 in. diameter black body hole.

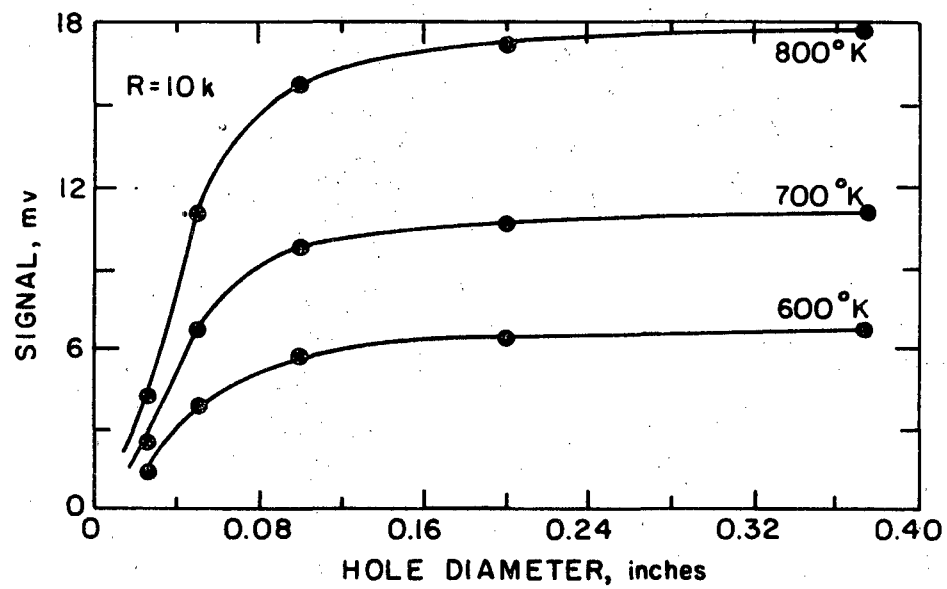

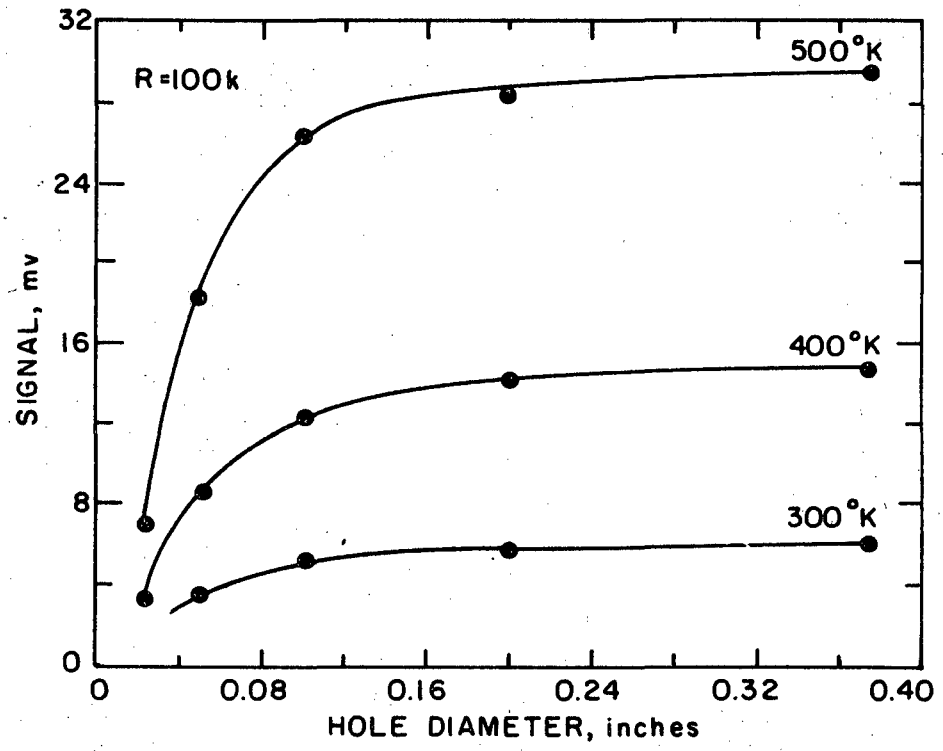

XBL 708-1900

Fig. 12. Pyrometer signal as function of black body hole diameter.

body hole, but not upon the temperature. The data of Fig. 12 can be correlated by the correction factors shown in the following table:

hole diameter, inches	Δ
0.100	0.133
0.156	0.065
0.200	0.045
0.375	0.000 (by definition)

All final calibrations were made with the 0.156 in. diam. hole on the black body sources (both above and below 1000°C).

The correction factor Δ was obtained for the black body holes of the commercial black body source. The holes of this source are surrounded by a surface essentially at room temperature, which contributes nothing to the signal. If, however, the black body hole is surrounded by a surface at a temperature which is appreciably greater than room temperature, an additional correction for this contribution to the total signal must be made. To make this correction, two measurements must be made. First the pyrometer is centered on the hole, and records a signal denoted by S_1. Then the pyrometer is focused on the area surrounding the hole (far enough away from the hole so that radiation from the hole is not received). This signal is denoted by S_2. If the surroundings are at room temperature or below, this signal is essentially zero.

Consider the signal S_1. It can be regarded as the sum of the signal due to a hole with room temperature surroundings, S_h, plus a

signal due to the warm surroundings, S_s:

$$S_1 = S_h + S_s \tag{12}$$

Now consider the signal due to the surroundings, S_s. This can be viewed as the difference between the signals that would be measured if: (i) the pyrometer viewed a large expanse of surface at the same temperature as the surroundings and (ii) the pyrometer viewed a disk of the surface of diameter equal to that of the black body hole but with the temperature and emissivity of the surroundings. The signal due to the large surface area ((i) above) is what is actually measured and is therefore equal to S_2. The signal due to the circular element is related to the signal from the large expanse of surface by Eq. (11). Thus, S_s may be written as:

$$S_s = S_2 - \frac{S_2}{1+\Delta} = \frac{\Delta}{1+\Delta} S_2 \tag{13}$$

Inserting Eq. (13) into Eq. (12), S_h is found to be:

$$S_h = S_1 - \left(\frac{\Delta}{1+\Delta}\right) S_2 \tag{14}$$

Thus, the two measurements S_1 and S_2 plus the hole size correction factor can be combined to determine what the signal would have been had the surroundings of the hole been at room temperature. The signal S_h can now be corrected by Eq. (11) to account for the difference in the diameter of the hole under consideration and the hole size for which the calibration curve was prepared (by multiplying by the factor $(1+\Delta)/(1+\Delta_c)$, where Δ_c is the correction factor for the calibration

hole and Δ is the correction factor for the measurement hole).

The procedure outlined above was needed to make the calibrations above 1000°C obtained with the graphite black bodies consistent with the calibration curve obtained below 1000°C with the commercial black body source. It is also necessary when measuring the temperature of black body holes with warm surroundings. Even if the surroundings are at the same temperature as the hole, they will appear cooler because the surface emissivity is less than the effective emissivity of the bottom of a hole.

E. Determination of Emissivity

If the surface and the hole are at the same temperature, and the hole has a length-to-diameter ratio sufficiently large to be considered a black body (or if it is in fact a cavity), the on-hole and off-hole measurements described in the preceding section can be utilized to determine the emissivity of the material. To accomplish this end, it must also be assumed that the spectral emissivity is independent of wave length over the 2 - 6μ bandpass of the detector (i.e., the body is gray over this range). If this is so, ε may be removed from the integral of Eq. (8). The integral then represents the current generated by a black body shining on the detector. The voltage across the detector (V of Eq. (10)) and hence the signal S, is simply proportional to the emissivity.

To determine the emissivity, assume the measurement S_1 and S_2 have been made and S_h computed by Eq. (14). S_2 represents the signal from a large surface at the same temperature as the black body hole but of emissivity ε instead of unity. S_h represents the signal from a black

body hole, which when multiplied by $1 + \Delta$, represents the signal which should have been observed if the hole were infinite in extent. The emissivity is simply the ratio of the signal from the infinite surface to that from the infinite black body hole:

$$\varepsilon = \frac{S_2}{(1+\Delta)S_h} = \frac{S_2}{(1+\Delta)S_1 - \Delta S_2} \tag{15}$$

If the hole is large ($\Delta \to 0$), $\varepsilon = S_2/S_1$.

F. Temperature Measurement of a Plane Surface

If the pyrometer is sighted on a large plane surface, the emissivity must be known if the temperature is to be obtained. If S_2 is the signal from the plane surface, S_2/ε is the signal which would have been measured had the surface been black. If the calibration of the pyrometer was performed on black body holes with cold surroundings and the hole size correction factor was Δ_c, $S_2/[\varepsilon(1+\Delta_c)]$ is the signal which would have been observed from a black body hole of the correct diameter and at the temperature of the plane surface under consideration. This quantity is used in conjunction with the calibration curves to determine the temperature of the surface.

IV. CALIBRATION

A. Below 1000°C

Below 1000°C the pyrometer was calibrated with an Infrared Industries model 404 black body. The black body source was itself calibrated with a calibrated thermocouple. The cavity emissivity was specified as 99% ± 1% and the control accuracy as ± 1°C. The calibration is shown in Fig. 13.

B. Above 1000°C

The two black body configurations shown in Fig. 14 - a cylindrical cavity and a cylindrical hole - were used for calibration above 1000°C. Both were constructed of graphite.

The graphite was heated in an induction heater. An argon flow was supplied to prevent oxidation. The graphite black body was then simultaneously viewed by the infrared pyrometer and an optical pyrometer as shown in Fig. 15. The high temperature calibration consisted of matching the corrected voltage output from the infrared pyrometer with the corresponding temperature measured by the optical pyrometer.

1. Emissivity of Hole

Because of the small solid angle subtended by the optical system, both the infrared and optical pyrometers view only the bottom of the hole. Sparrow, Albers and Eckert[6] have calculated the effective emissivity of the bottom of cylindrical holes with gray, diffusely emitting surfaces. For a hole of length to diameter ratio of 4 in a material of emissivity 0.5, the effective emissivity of the bottom of the hole is 0.988.[6] Since the emissivity of graphite[7] is greater than 0.5 between 0.65μ and 6μ, (the range at which both the

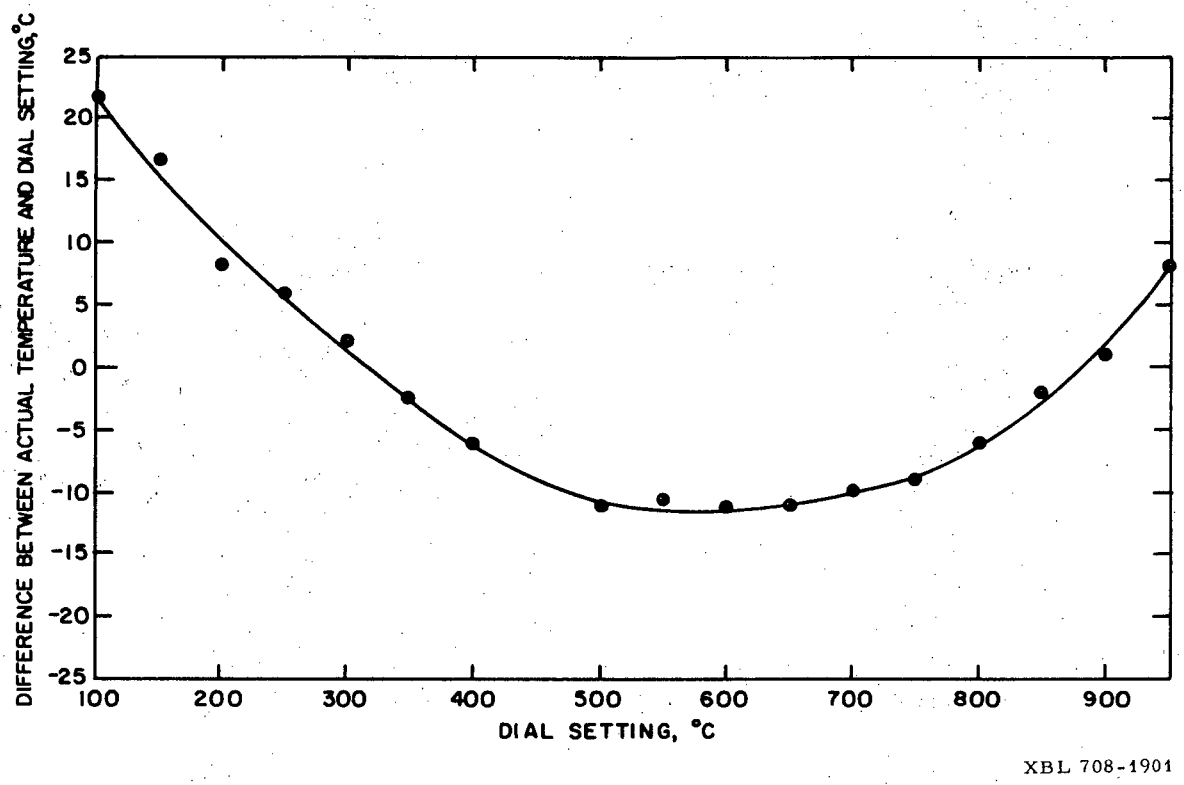

Fig. 13. Temperature calibration of commercial black body source.

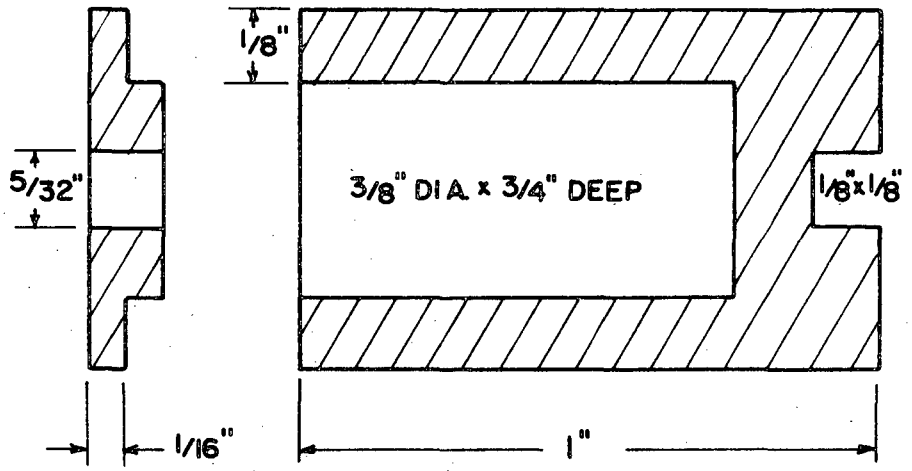

BLACK BODY CAVITY

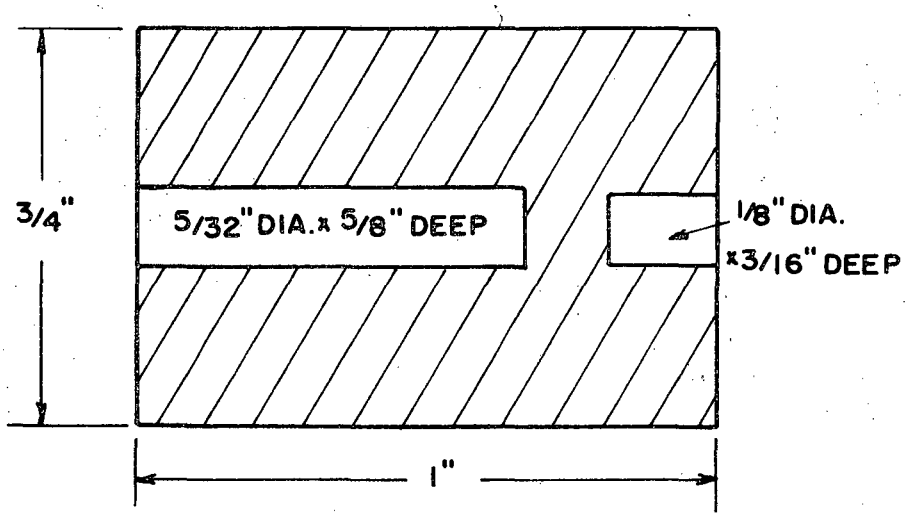

BLACK BODY HOLE

XBL 708-1899

Fig. 14. Graphite black body sources used for calibration above 1000°C.

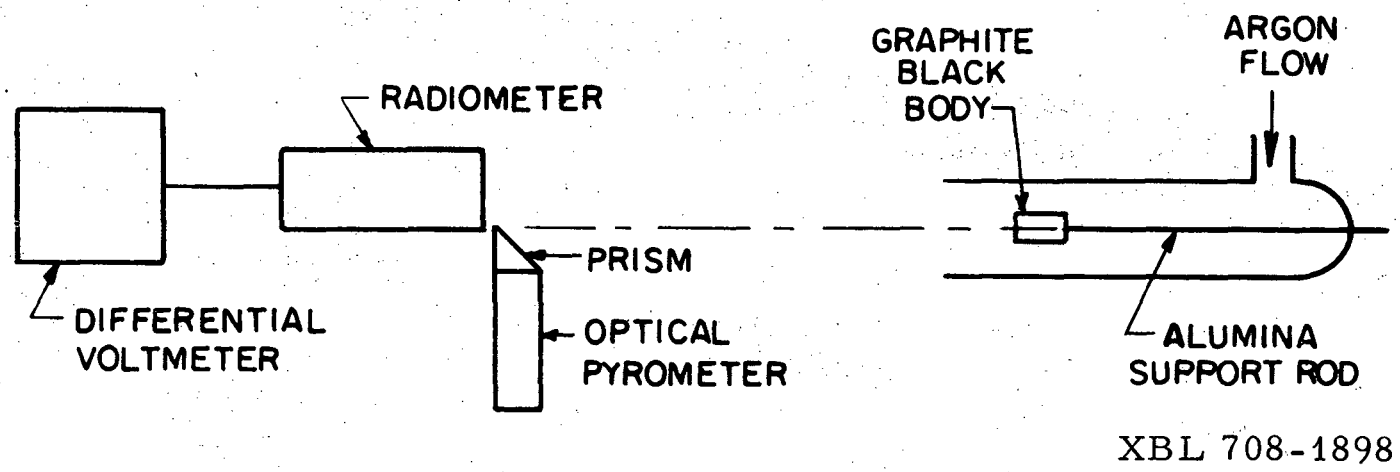

Fig. 15. Setup for calibration above 1000°C.

optical and infrared pyrometers are sensitive), a cylindrical hole in graphite is an excellent approximation to a black body.

2. Emissivity of Cavity

Quinn[8] has calculated the emissivity of cylindrical cavities closed at one end and having an opening on the other end equal to or smaller than the radius of the cylinder.

For the cavity shown in Fig. 14 with surfaces of emissivity of 0.5, a minimum value of 0.987 was calculated for the emissivity of the bottom of the cavity (which is viewed by the pyrometer).

3. Non-Blackness Correction

For the optical pyrometer, the relationship between the brightness temperature (T_{app}) and the true temperature (T) is

$$\frac{1}{T_{app}} - \frac{1}{T} = -\left(\frac{\lambda}{C_2}\right) \ln \varepsilon \qquad (16)$$

Where $\lambda = 0.65\mu$ and C_2, Planck's second radiation constant, equals 1.438 cm/°K. An emissivity of 0.988 will yield a correction to the brightness temperature of 0.6°K at 1000°K, and 2.4°K at 2000°K. A correction of this magnitude is insignificant since it lies within the range of accuracy of the optical pyrometer.

For the infrared pyrometer, operating under conditions that Eq. (10) is valid, the measured signal should be increased by ~1.2% to account for an effective emissivity of 0.988 (assuming the body is gray). This small correction has been neglected in the calibrations.

C. Calibration Conditions

The calibration curves obtained with the black-body sources are shown in Appendix B. These curves were obtained with black body holes of 0.156 in. diam. With the commercial source, the surface adjacent to the hole was at room temperature. Two readings were made on the graphite black-body sources; one on the hole and one on the surface adjacent to the hole. These two results and Eq. (14) were used to correct the measurement to what would have been obtained if the surroundings of the hole had been cool. In this manner the calibration from the commercial black body and the graphite black bodies were both placed on the same basis. When the calibration curves are used to determine temperatures from measurements of pyrometer output, care must be taken to correct for:

1. Emissivity of the material
2. Size of hole (if different from 0.156 in. diameter)
3. Temperature of the surface adjacent to the hole

The calibrations are valid only for 24 in. between source and pyrometer. At other distances, the curve of Fig. 8 may be used to correct readings to 24 in., but with loss of accuracy.

To avoid the saturation problem shown in Fig. 5, the system was calibrated for three load resistors: 100k up to 500°C; 10k from 500°C to 1200°C and 1k for higher temperatures. The actual load resistance in the circuit of Fig. 2 is less than these values because of the oscilloscope and digital voltmeter, whose 1M imput resistances were in parallel with R. Thus, the calibration curves refer to load resistances given by:

$$\frac{1}{R_{act}} = \frac{1}{R} + \frac{2}{10^6}$$

V. THEORETICAL OUTPUT VS. TEMPERATURE

It is of interest to ascertain whether the calibration curves of Appendix B show the expected variation of signal strength with source temperature. The connection between these two quantities was developed in Sec. II-B.

If the infrared pyrometer is operated in the range where Eq. (10) is valid, the output signal is proportional to the integral of Eq. (8). Using Eq. (9) for the detector response function and approximating the black body spectrum by Eq. (2), Eq. (8) may be integrated analytically to yield:

$$S = \frac{K}{\lambda_{max}^4} \exp\left(-\frac{1}{\alpha_{max}}\right)\left[\alpha_{max}+3\alpha_{max}^2+6\alpha_{max}^3+6\alpha_{max}^4\right] - \frac{K}{\lambda_{min}^4} \exp\left(-\frac{1}{\alpha_{min}}\right)\left[\alpha_{min}+3\alpha_{min}^2+6\alpha_{min}^3+6\alpha_{min}^4\right] \tag{17}$$

$$\text{where } \alpha_{max} = \frac{\lambda_{max}}{\left(a+\frac{C_2}{T}\right)}, \quad \alpha_{min} = \frac{\lambda_{min}}{\left(a+\frac{C_2}{T}\right)}$$

Figs. 16 and 17 present a comparison between Eq. (17) and the measurements in both the high and low temperature regions. The constant of proportionality K was determined by matching a measurement with Eq. (17) at a convenient temperature. Values of $\lambda_{min} = 2\mu$, $\lambda_{max} = 5.2\mu$ and $a = 0.3\mu$ were used. These parameters (which are not known accurately) may be slightly varied to obtain a closer match of theory and experiment. At high temperatures, better agreement would have been obtained if Planck's law, Eq. (1), were used instead of Wien's approximation, Eq. (2).

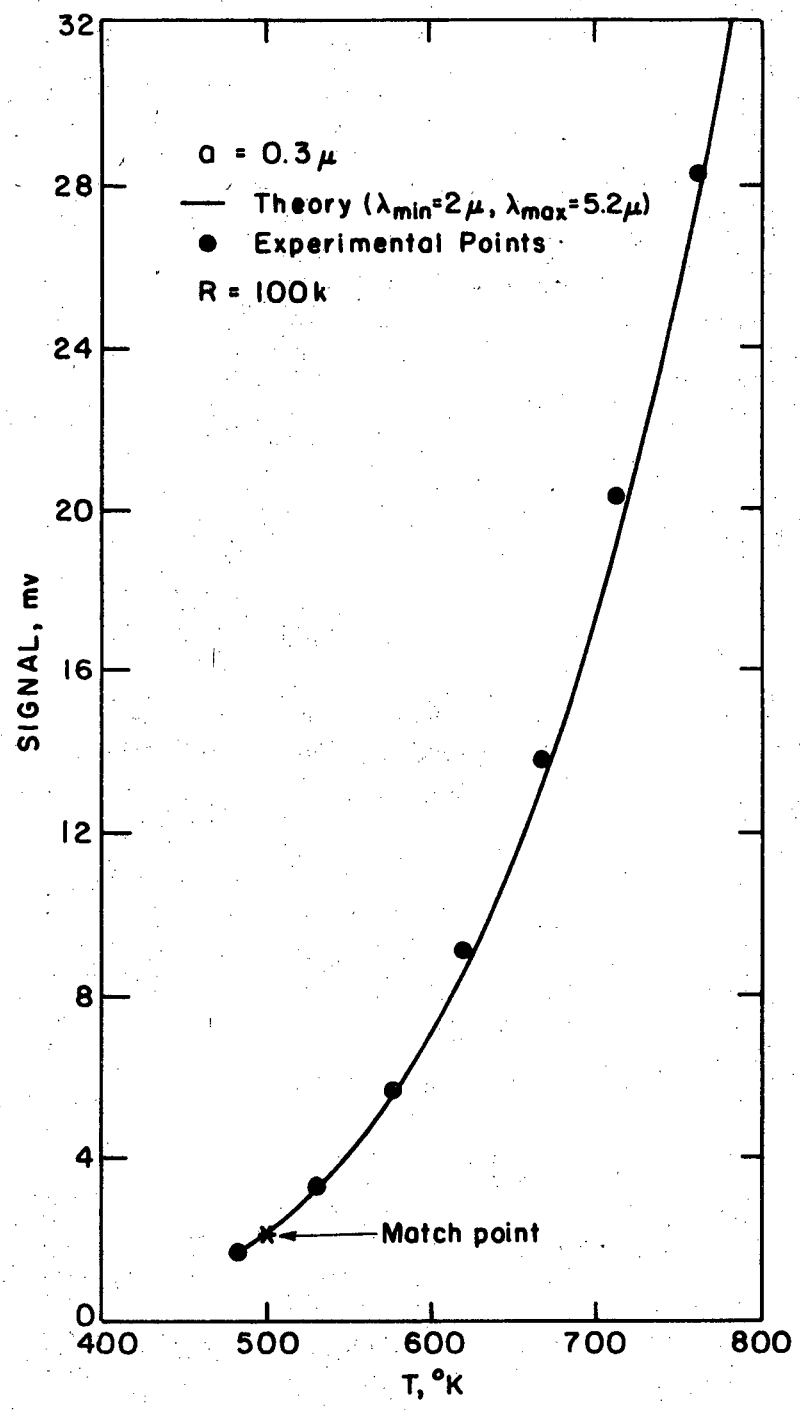

XBL 708-1897

Fig. 16. Comparison between measured and calculated signal at low temperatures.

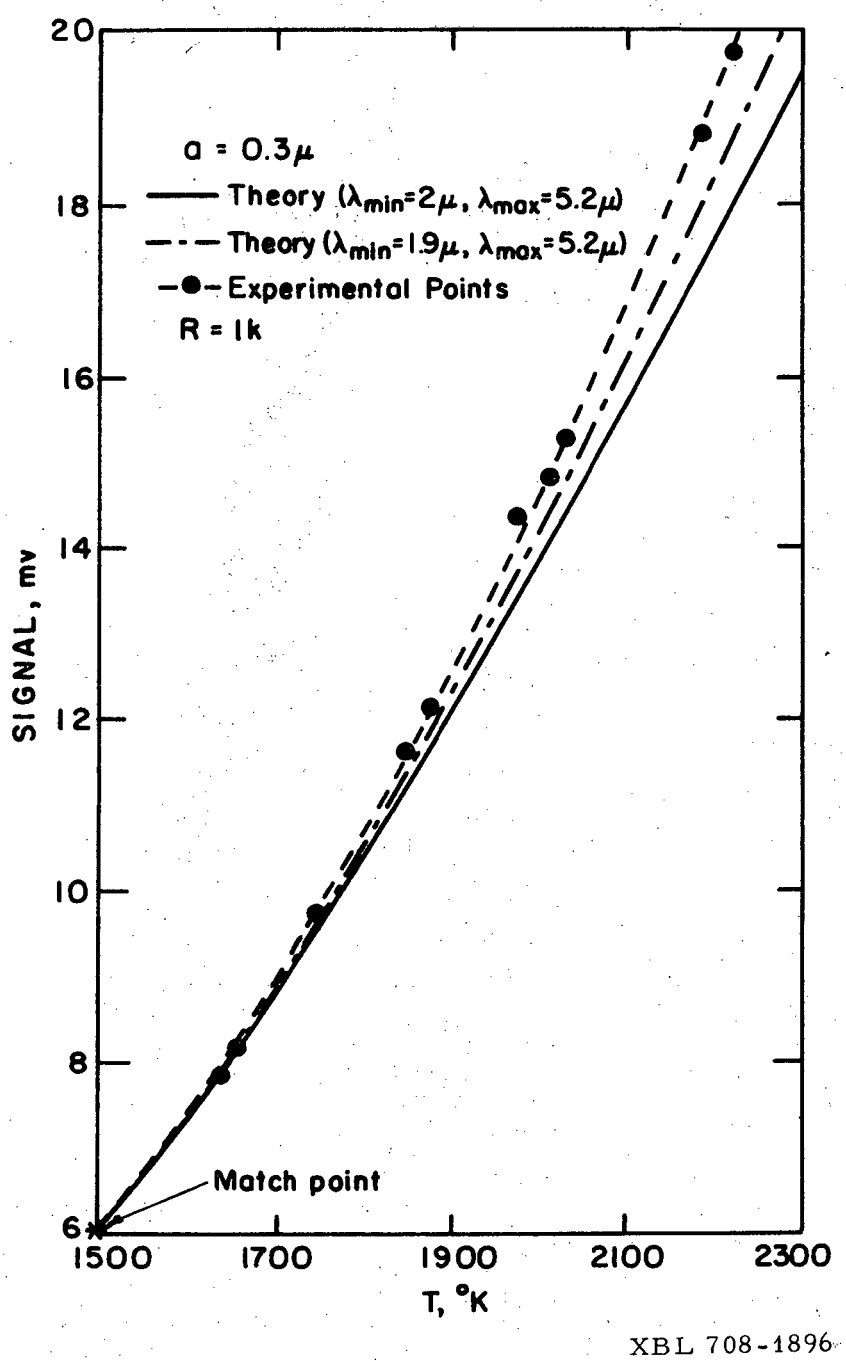

Fig. 17. Comparison between measured and calculated signal at high temperatures.

Figures 18 and 19 show that the data are closely approximated by a straight line on a plot of the logarithm of the signal versus the reciprocal temperature. Therefore, an equation of the form: $S = S_0 \exp(-A/T)$ may be utilized for extrapolation to temperatures beyond the upper limit of the calibrations performed here.

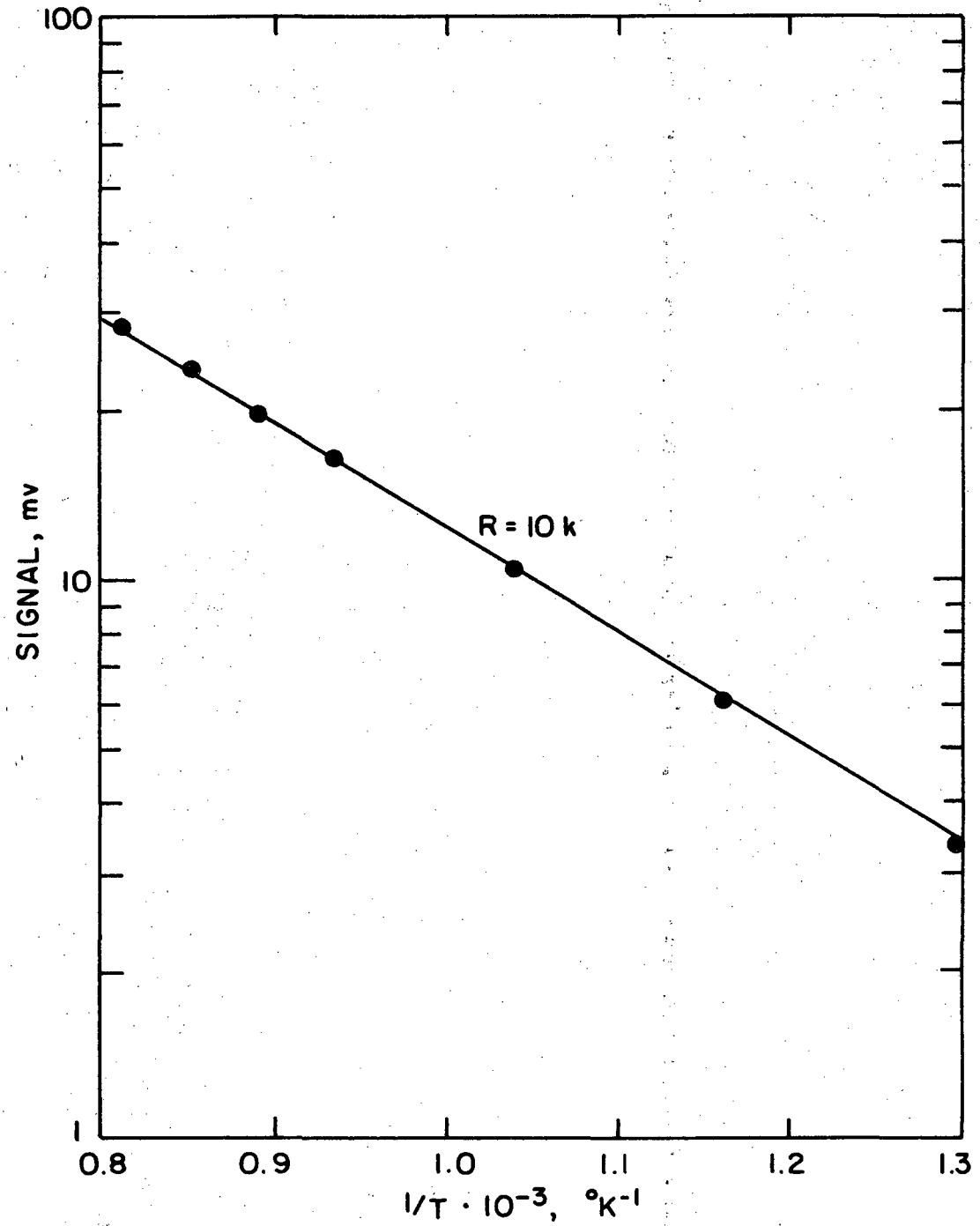

XBL 708-1895

Fig. 18. Logarithm of measured signal vs. reciprocal temperature for 10K scale.

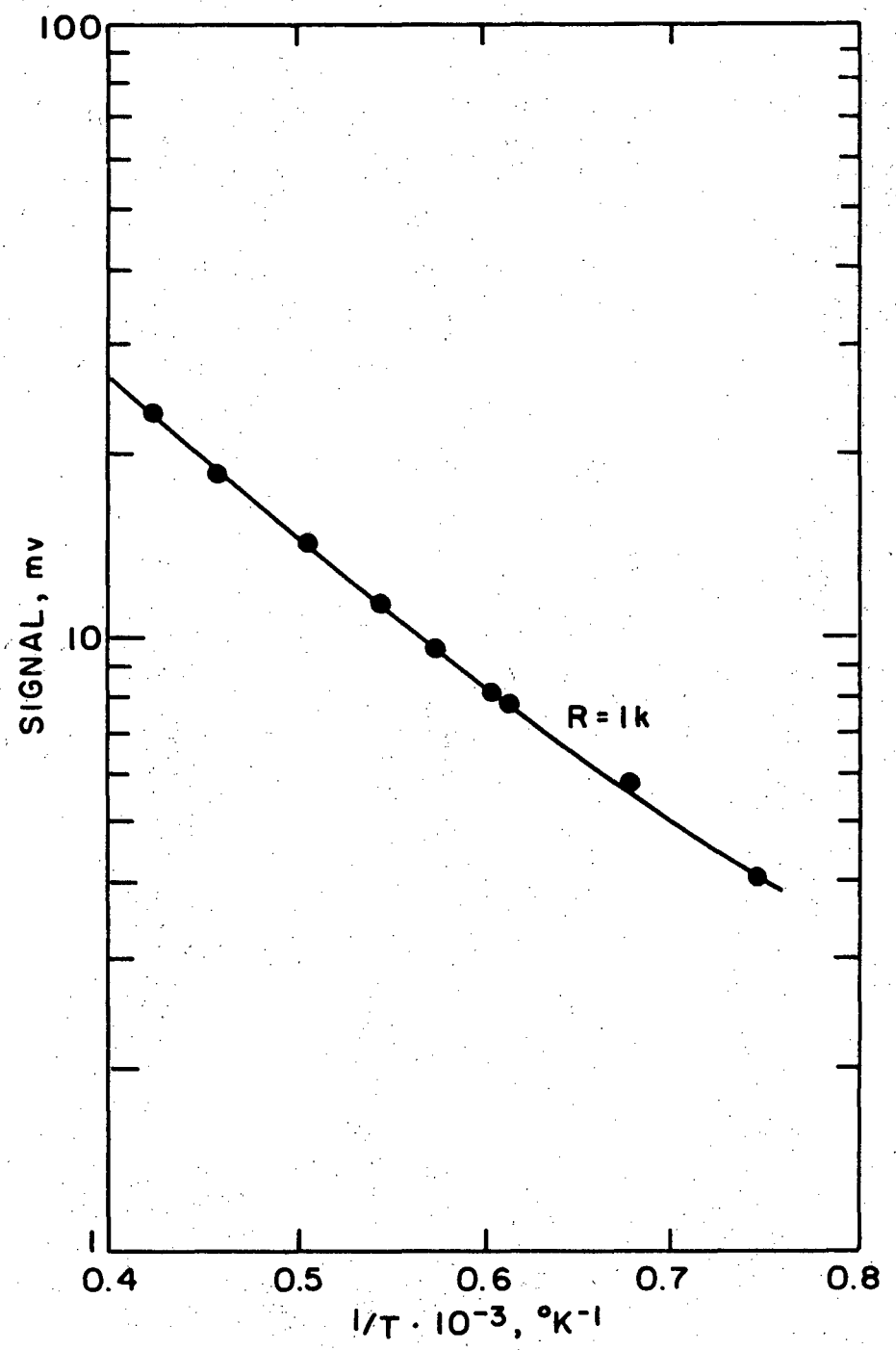

XBL 708-1894

Fig. 19. Logarithm of measured signal vs. reciprocal temperature of 1K scale.

VI. RESPONSE TIME

The time constant of an infrared detector is generally determined by the square pulse technique. Square pulses of radiation can be obtained by reflecting radiation from a rotating mirror onto the detector.

Lacking the optics necessary for the square radiation pulse technique, the electrical analog shown in Fig. 20 was used.[3] The time constant measured was the RC time constant of the signal-processing circuit rather than the time constant determined by the transit time of the charge carriers of the photodiode. It was assumed that the diode capacitance for incident light was the same as that for an applied voltage and that the capacitance was independent of the magnitude of the applied voltage.

A square wave generator was used to provide input pulses of rise and fall time less than .1μ sec. When 0.03 or 0.06 volts was applied across the circuit of Fig. 20, the following response times were measured

$$\tau = 1.4\mu \text{ sec with diode in circuit}$$

$$\tau_0 = 0.7\mu \text{ sec without diode in circuit.}$$

According to Fig. 20,

$$\tau_0 = C_s \left(\frac{1}{\frac{1}{R_1} + \frac{1}{R_2} + \frac{1}{R_s}} \right)$$

where C_s is the capacitance of the oscilloscope and stray capacitance in connecting cables. Therefore,

$$C_s = 80\text{pf}.$$

with the diode in the circuit,

$$\tau = (C_s + C_{diode}) \left[\frac{1}{\frac{1}{R_1} + \frac{1}{R_2} + \frac{1}{R_{diode}} + \frac{1}{R_s}} \right]$$

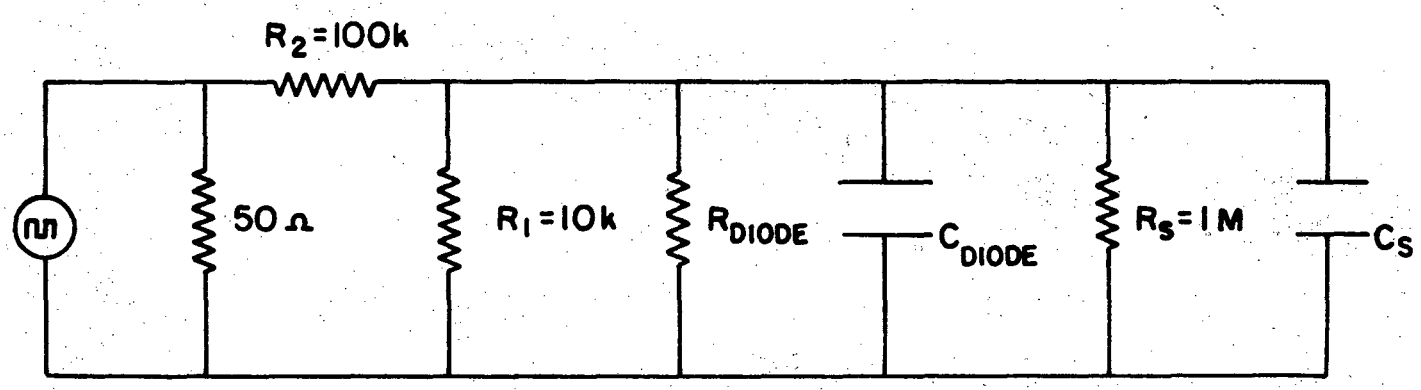

XBL 708-1893

Fig. 20. Circuit for measuring system response time.

R_{diode} was measured as 20 M. Therefore

$$C_{diode} = 80 \text{ pf.}$$

The time constant of an RC circuit is simply RC. For the actual detector circuit R is the net parallel resistance of R_{diode} and the resistance used in the circuit of Fig. 2. The time constant for the detector is:

0.08μ sec for 1k

0.8 μ sec for 10k

8 μ sec for 100k

Stray capacitance has been neglected in these estimates. For measurement of rapid temperature transients, the chopper in Fig. 6 is removed and the signal is measured on an oscilloscope.

Acknowledgments

This work was done under the auspices of the U. S. Atomic Energy Commission.

APPENDIX A

CASSEGRAIN LENS SYSTEM: THEORETICAL SPOT SIZE

The paraxial ray equation for a mirror is:[9]

$$\frac{1}{S} - \frac{1}{S'} = -\frac{2}{R}$$

where S = source to mirror distance

S'= mirror to image distance

R = mirror radius

For the configuration shown in Fig. 21,

$$\frac{1}{S_1} - \frac{1}{S_1'} = \frac{2}{R_1} \qquad \text{(A-1)}$$

and

$$\frac{1}{S_2} = -\frac{2}{R_2} \qquad \text{(A-2)}$$

since S_2' is infinite for the convex mirror because the beam produced by it is parallel to the optical axis. Since both S_2 and S_1' on Fig. 21 are negative,

$$S_2 = S_1' + D \qquad \text{(A-3)}$$

the above equations give:

$$\frac{1}{S_1} + \frac{1}{\frac{R_2}{2} + D} = \frac{2}{R_1} \qquad \text{(A-4)}$$

The problem is to calculate the focal spot radius, h_{min}, for which all of the rays emitted from h_{min} and incident on the concave mirror also impinge on the convex mirror and are eventually detected. It is assumed that the requirements are just met for a ray impinging on the far side of the concave mirror which barely intercepts the convex mirror.

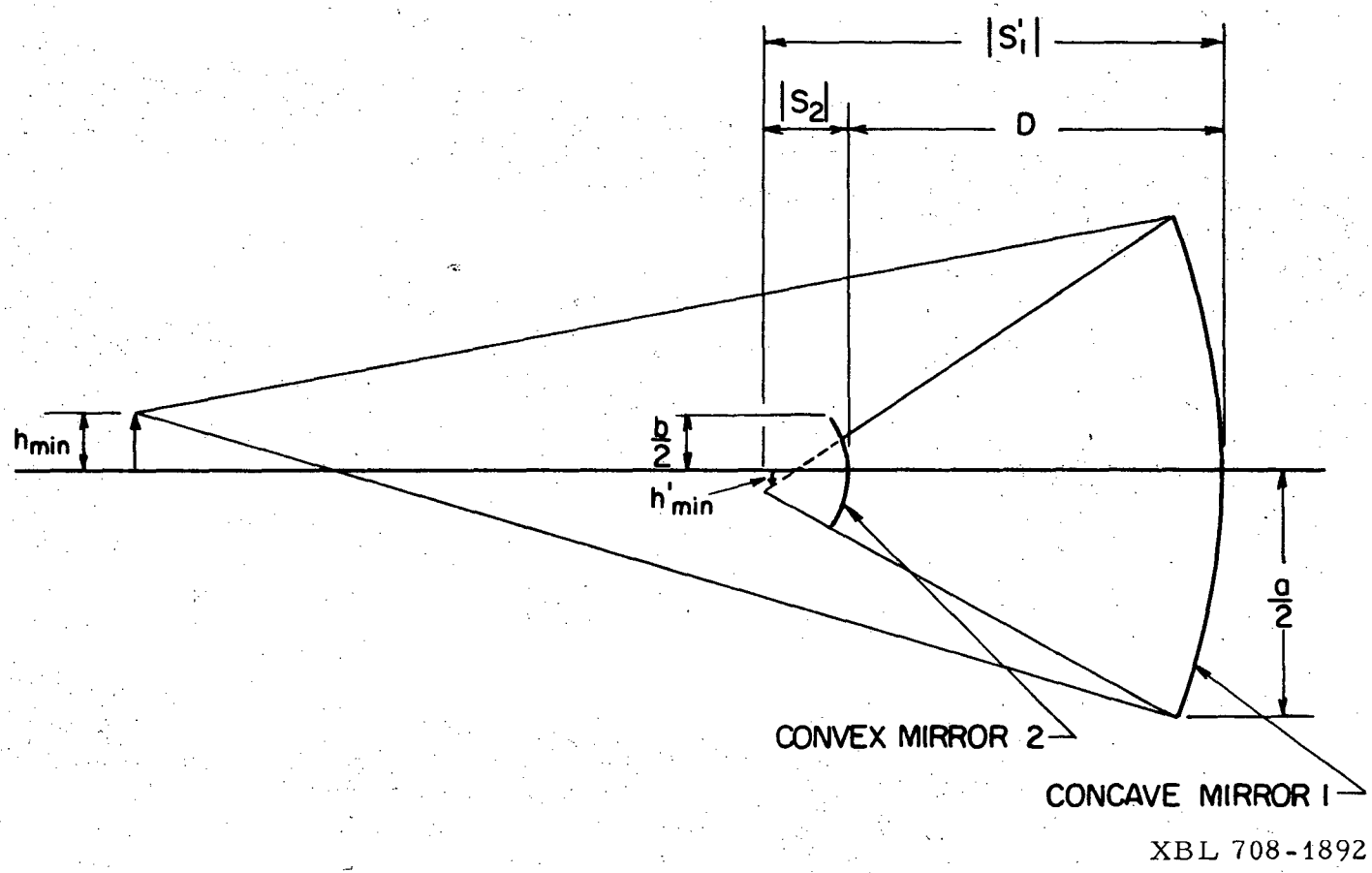

Fig. 21. Mirror geometry for spot size calculation.

Consider the bottom ray in Fig. 21 and its reflection from the concave mirror. By examination of the relationships among the pertinent dimensions:

$$\frac{h'_{min}}{x} = \frac{b/2}{x + |S_2|} = \frac{a/2}{D + |S_2| + x} \qquad \text{(A-5)}$$

where h'_{min} is the image height of h_{min} formed by the concave mirror and x is the distance along the axis between h'_{min} and the intersection of reflected bottom ray with the axis.

Using Eq. (A-2) yields:

$$h'_{min} = \frac{b}{2} - \frac{R_2(a-b)}{4D} \qquad \text{(A-6)}$$

The magnification of the optical system is given by:

$$m = -\frac{h'}{h} = \frac{S_1'}{S_1} \qquad \text{(A-7)}$$

Therefore with S_1' from (A-2) and (A-3):

$$h_{min} = h'_{min}\, S_1 / \frac{R_2}{2} + D \qquad \text{(A-8)}$$

or substituting h'_{min} from (A-6):

$$h_{min} = \frac{S_1}{\frac{R_2}{2} + D} \quad \frac{b}{2} - \frac{R_2(a-b)}{4D} \qquad \text{(A-9)}$$

Following the same type of procedure for h_{max} (not shown on Fig. 21), the focal spot radius at which no emitted rays falling on the concave mirror may be detected, gives:

$$h_{max} = \frac{S_1}{\frac{R_2}{2} + D} \quad \frac{b}{2} + \frac{R_2(a+b)}{4D} \qquad \text{(A-10)}$$

By making various measurements on the optical system it was found that:

$a = 1.3''$

$b = 0.25''$

$R_1 = 12''$

$R_2 = 2.5''$

$D = 6.2''$

Utilizing these numbers, S_1 was calculated from (A-4) to be 31 in., which corresponds to a normal 24 in. source-detector distance. Values of $h_{min} = 0.058''$ and $h_{max} = 1.14$ in. were calculated. Therefore, when the pyrometer is calibrated at 24 in., all of the radiation falling on the concave lens within a focal spot radius of 0.058" will be detected. A part of the radiation falling on the concave lens up to a spot radius of 1.14 inches will be detected.

These results are expected to overestimate the spot size since not all of the rays incident on the convex mirror are actually detected.

APPENDIX B

CALIBRATION CURVES

For a 0.156 in. black body hole with room temperature surroundings at a distance of 24 in. Also see note concerning load resistances in Sec. IV-C.

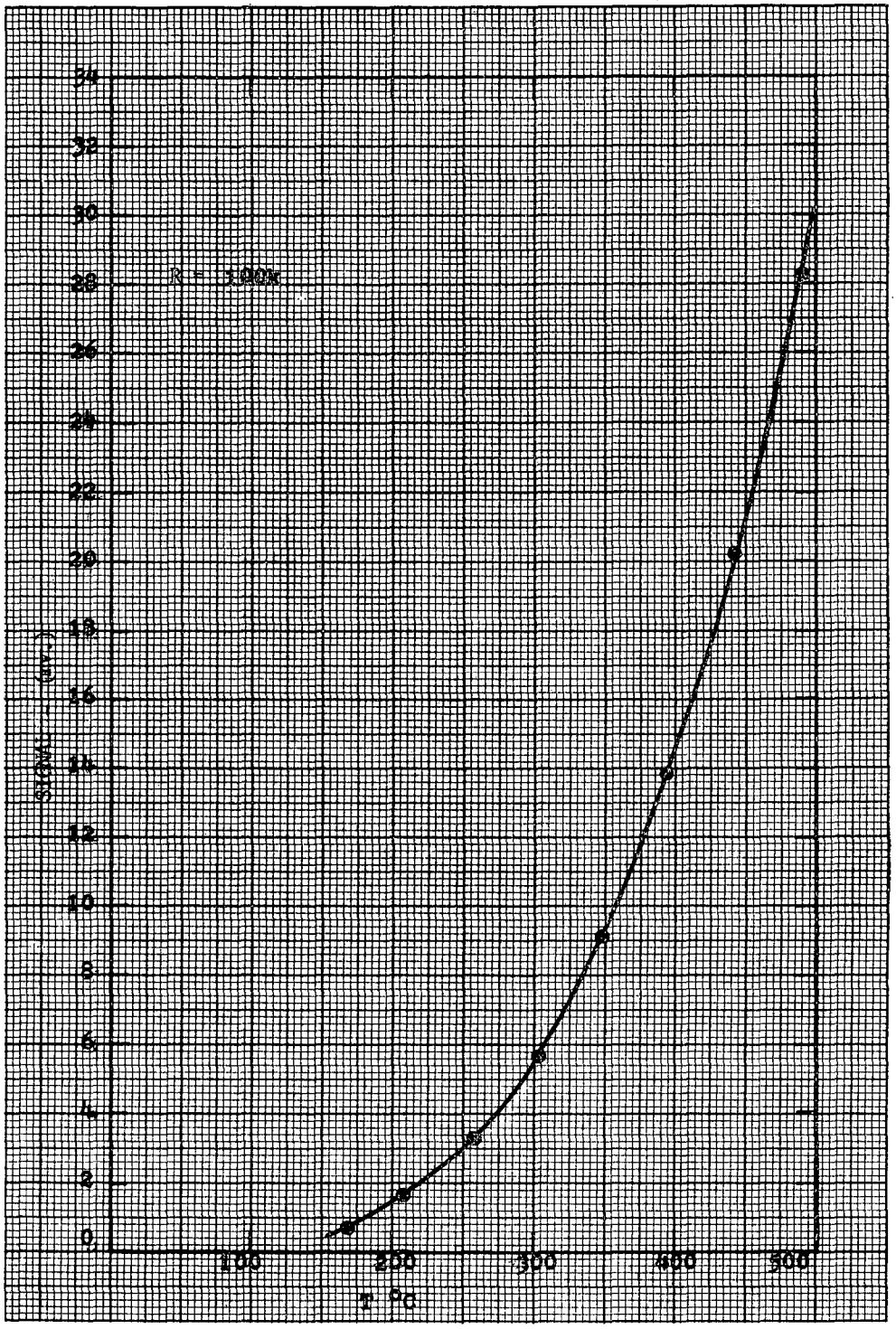
R = 100K
SIGNAL - (mv.)
T °C
0
2
4
6
8
10
12
14
16
18
20
22
24
26
28
30
32
34
100
200
300
400
500

XBL 708-6405

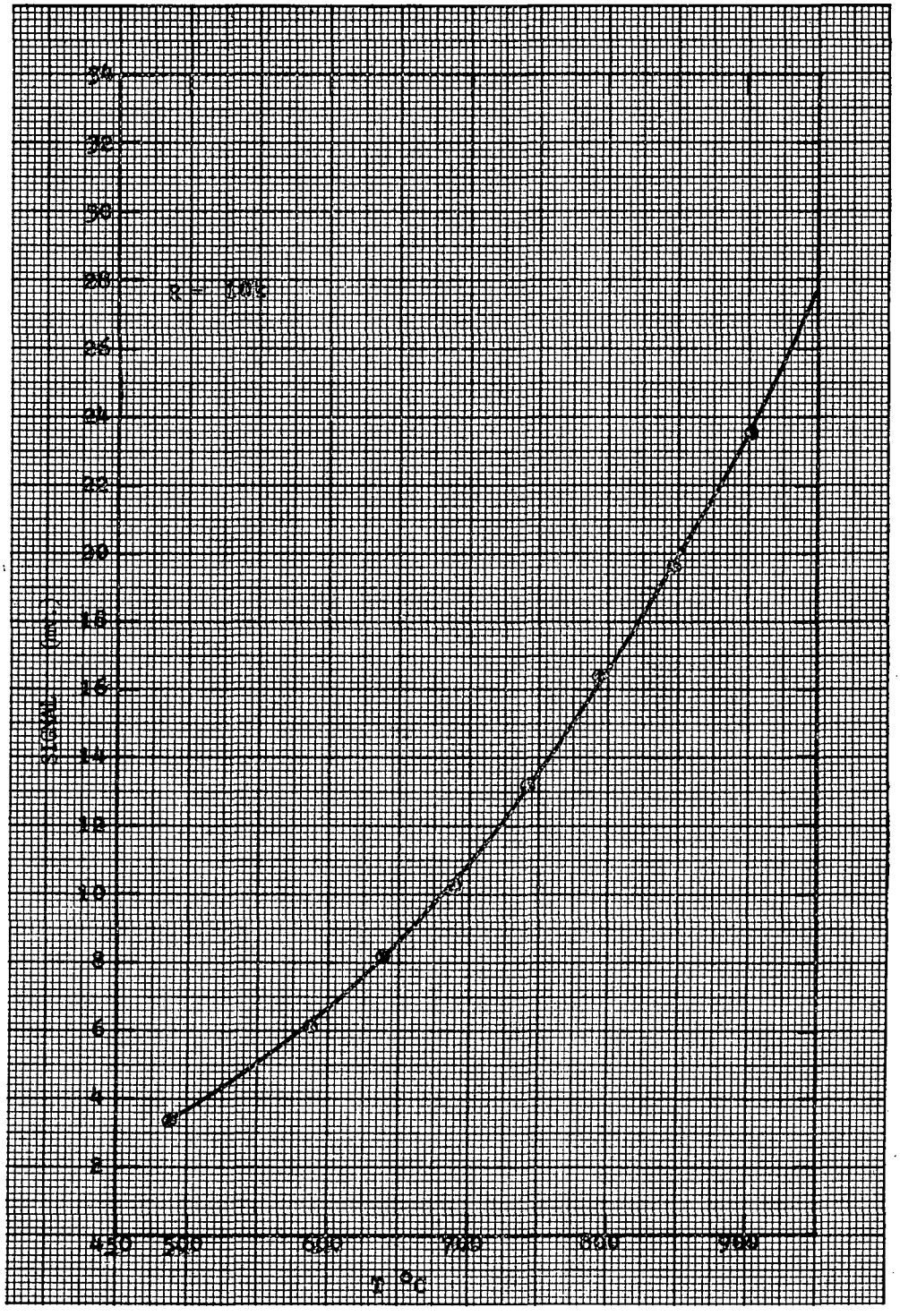
34
32
30
28
26
24
22
20
18
16
14
12
10
8
6
4
2
SIGNAL (mv)
450
500
600
700
800
900
T °C

XBL 708-6402

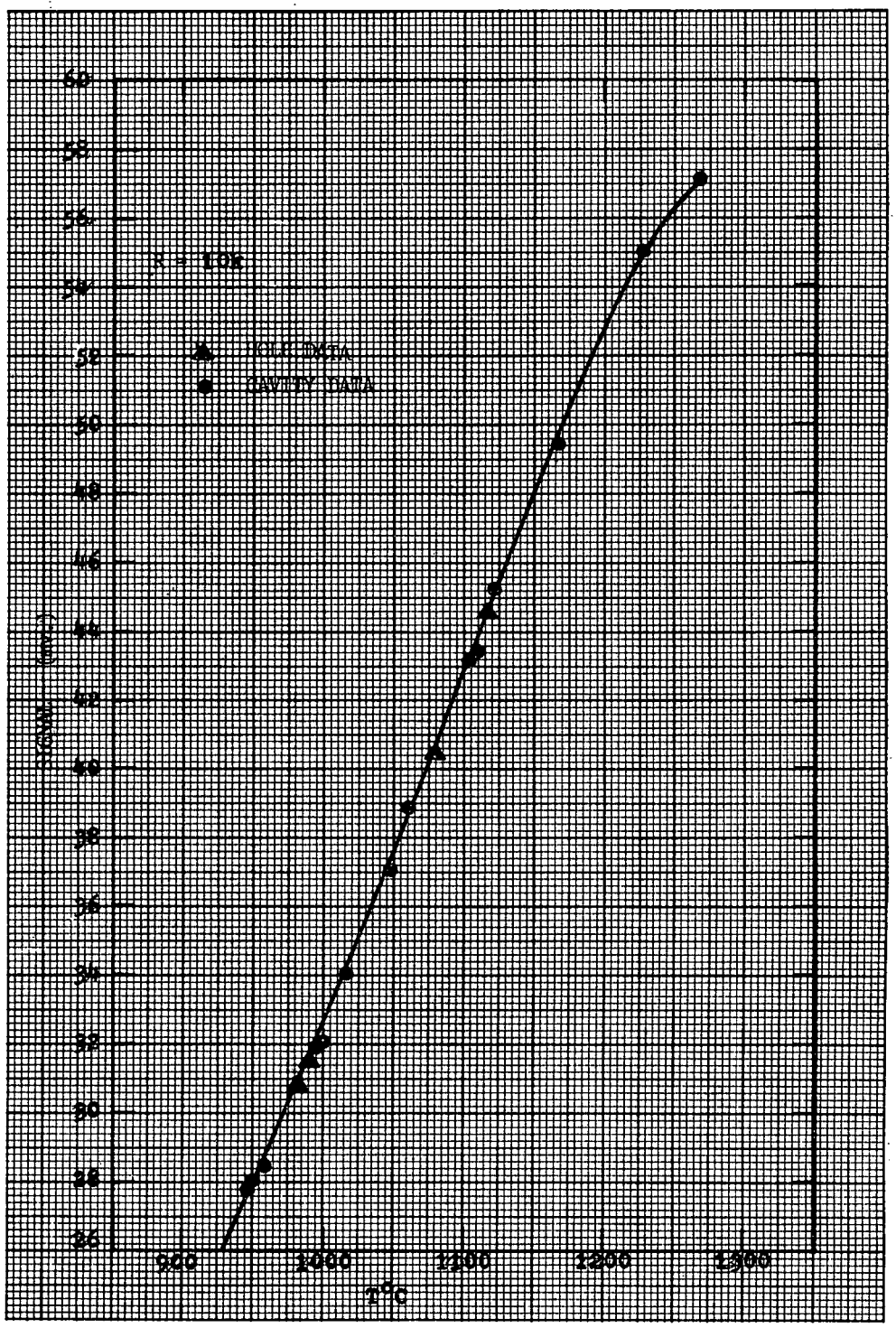
R = 10k
HOLE DATA
CAVITY DATA
SIGNAL (mv.)
60
58
56
54
52
50
48
46
44
42
40
38
36
34
32
30
28
26
900
1000
1100
1200
1300
T°C

XBL 708-6403

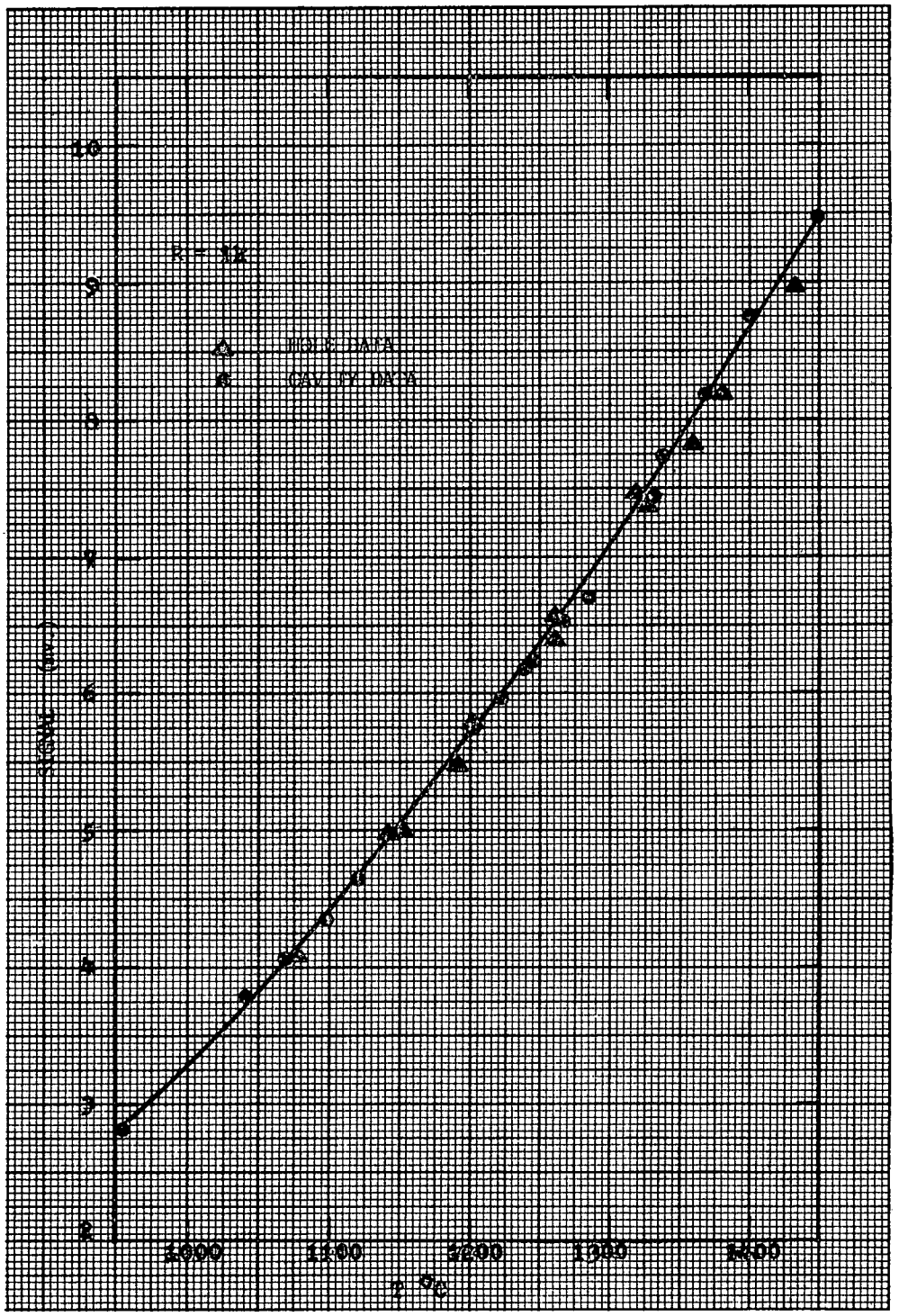
R = 1k
HOLE DATA
CAVITY DATA
SIGNAL (mv)
10
9
8
7
6
5
4
3
2
1000
1100
1200
1300
1400
T °C

XBL 708-6404

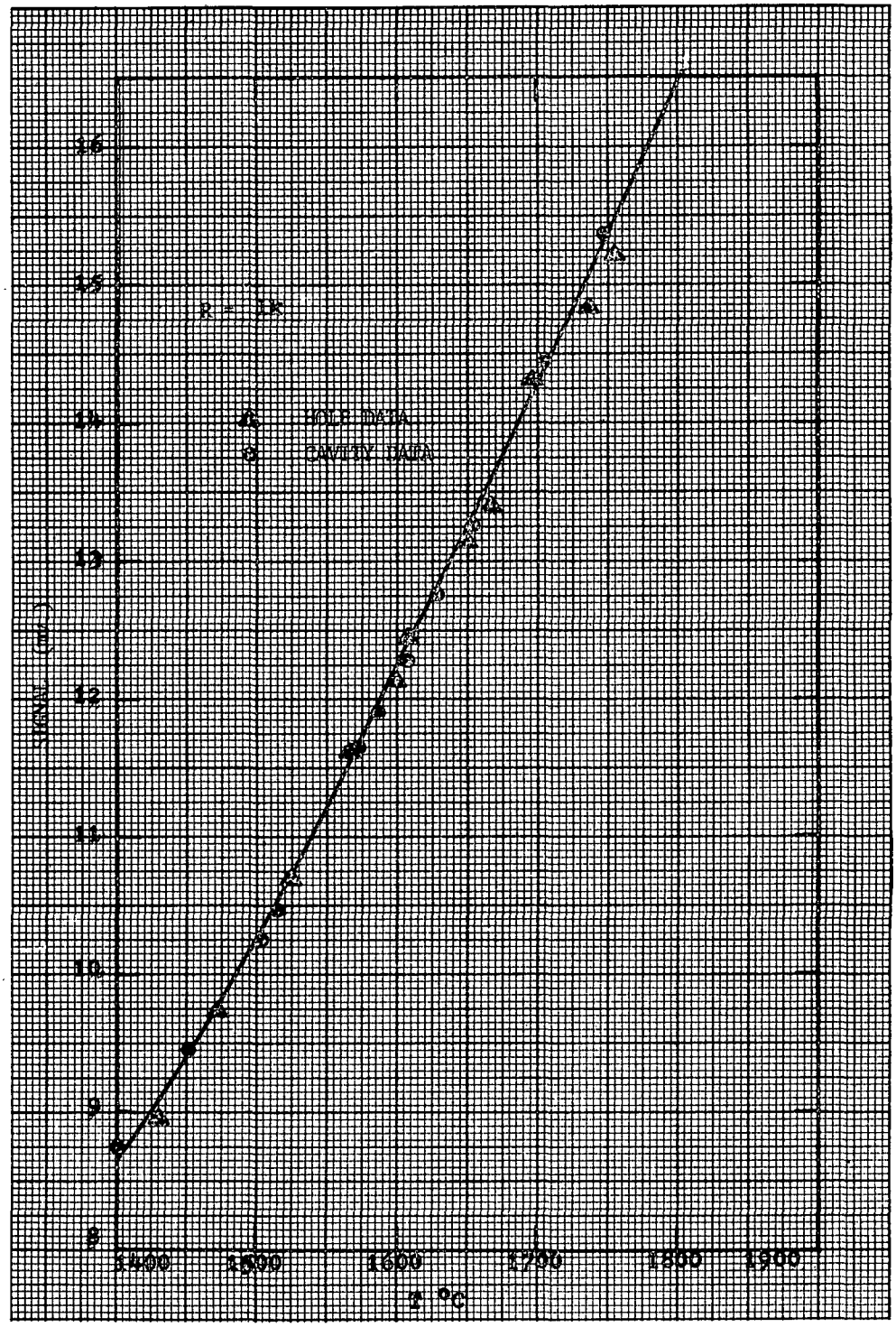
16
15
14
13
12
11
10
9
8
SIGNAL (mv)
R = 1K
HOLE DATA
CAVITY DATA
1400
1500
1600
1700
1800
1900
T °C

XBL 708-6401

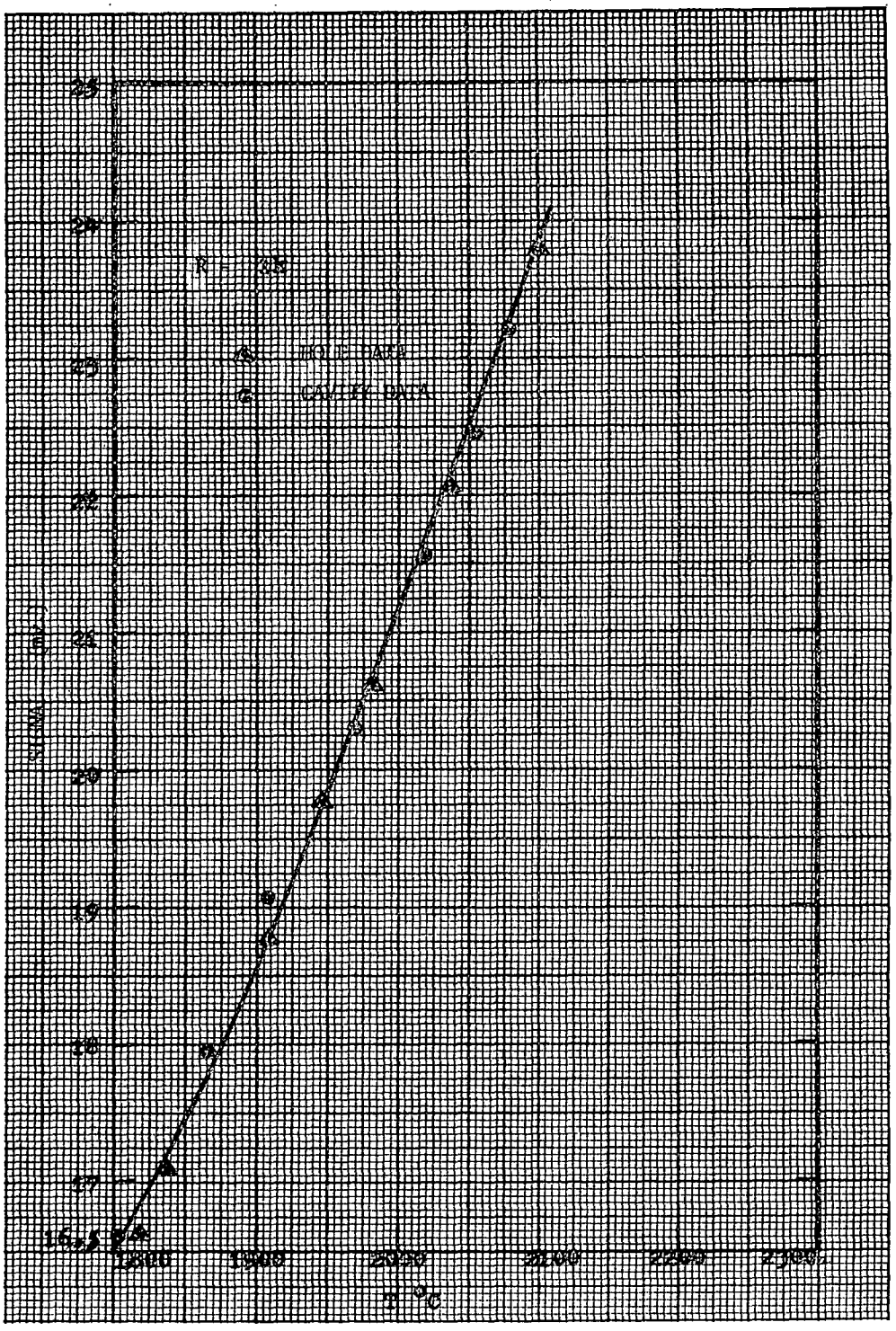
HOLE DATA
CAVITY DATA
25
24
23
22
21
20
19
18
17
16.5
1800
1900
2000
2100
2200
2300
T °C

XBL 708-6406

BIBLIOGRAPHY

1. Wilson, R. E., et al., Temperature Measurement and Control Handbook, reprint from Instruments and Control Systems, Chilton Company, Pittsburgh, Pa., 1966.

2. Kingslake, R., ed., Applied Optics and Optical Engineering, Academic Press, New York, 1965, Chapter 8.

3. Pederson, D. O., J. J. Studer, and J. R. Whinnery, Introduction to Electronic Systems, Circuits, and Devices, McGraw-Hill Book Company, New York, 1964, Chaps. 7 and 12.

4. Philco-Ford Corp., Product Sheet EO-100 (April 1969).

5. Philco-Ford Corp., Application Note #175.

6. Sparrow, E. M., L. U. Albers, E. R. G. Eckert, "Thermal Radiation Characteristics of Cylindrical Enclosures," J. Heat Transfer, Transactions of the ASME Series C, 84, 73, (1962).

7. Autio, G. W., and E. Scala, "Normal Spectral Emissivity of Isotropic and Anisotropic Materials," AIAA Journal, 3, 738, (1965).

8. Quinn, T. J., "The Calculation of the Emissivity of Cylindrical Cavities Giving Near Black-Body Radiation," Brit. J. Appl. Phys., 18, 1105, (1967).

9. Sears, F. W., Optics, Addison-Wesley Publishing Company, Reading, Mass., 1949, p. 68.

LEGAL NOTICE

This report was prepared as an account of Government sponsored work. Neither the United States, nor the Commission, nor any person acting on behalf of the Commission:

A. Makes any warranty or representation, expressed or implied, with respect to the accuracy, completeness, or usefulness of the information contained in this report, or that the use of any information, apparatus, method, or process disclosed in this report may not infringe privately owned rights; or

B. Assumes any liabilities with respect to the use of, or for damages resulting from the use of any information, apparatus, method, or process disclosed in this report.

As used in the above, "person acting on behalf of the Commission" includes any employee or contractor of the Commission, or employee of such contractor, to the extent that such employee or contractor of the Commission, or employee of such contractor prepares, disseminates, or provides access to, any information pursuant to his employment or contract with the Commission, or his employment with such contractor.

TECHNICAL INFORMATION DIVISION
LAWRENCE RADIATION LABORATORY
UNIVERSITY OF CALIFORNIA
BERKELEY, CALIFORNIA 94720